Development/Plasticity/Repair

Structure of Long-Range Direct and Indirect Spinocerebellar Pathways as Well as Local Spinal Circuits Mediating Proprioception

Iliodora V. Pop,[1] Felipe Espinosa,[1] Cheasequah J. Blevins,[2,3] Portia C. Okafor,[1] Osita W. Ogujiofor,[1] Megan Goyal,[1] Bishakha Mona,[1] Mark A. Landy,[1] Kevin M. Dean,[4] Channabasavaiah B. Gurumurthy,[5,6] and Helen C. Lai[1]

[1]Department of Neuroscience, UT Southwestern Medical Center, Dallas, Texas 75390, [2]Mathematical Biosciences Institute, Ohio State University, Columbus, Ohio 43210, [3]Department of Physiology and Biophysics, University of Colorado School of Medicine, Aurora, Colorado 80045, [4]Lyda Hill Department of Bioinformatics, UT Southwestern Medical Center, Dallas, Texas 75390, [5]Mouse Genome Engineering Core Facility, University of Nebraska Medical Center, Omaha, Nebraska 68198, and [6]Department of Pharmacology and Experimental Neuroscience, College of Medicine, University of Nebraska Medical Center, Omaha, Nebraska 68198

Proprioception, the sense of limb and body position, generates a map of the body that is essential for proper motor control, yet we know little about precisely how neurons in proprioceptive pathways are wired. Defining the anatomy of secondary neurons in the spinal cord that integrate and relay proprioceptive and potentially cutaneous information from the periphery to the cerebellum is fundamental to understanding how proprioceptive circuits function. Here, we define the unique anatomic trajectories of long-range direct and indirect spinocerebellar pathways as well as local intersegmental spinal circuits using genetic tools in both male and female mice. We find that Clarke's column neurons, a major contributor to the direct spinocerebellar pathway, has mossy fiber terminals that diversify extensively in the cerebellar cortex with axons terminating bilaterally, but with no significant axon collaterals within the spinal cord, medulla, or cerebellar nuclei. By contrast, we find that two of the indirect pathways, the spino-lateral reticular nucleus and spino-olivary pathways, are in part, derived from cervical *Atoh1*-lineage neurons, whereas thoracolumbar *Atoh1*-lineage neurons project mostly locally within the spinal cord. Notably, while cervical and thoracolumbar *Atoh1*-lineage neurons connect locally with motor neurons, no Clarke's column to motor neuron connections were detected. Together, we define anatomic differences between long-range direct, indirect, and local proprioceptive subcircuits that likely mediate different components of proprioceptive-motor behaviors.

Key words: Atoh1; cerebellum; Clarke's column; proprioception; spinal cord; spinocerebellar

Significance Statement

We define the anatomy of long-range direct and indirect spinocerebellar pathways as well as local spinal proprioceptive circuits. We observe that mossy fiber axon terminals of Clarke's column neurons diversify proprioceptive information across granule cells in multiple lobules on both ipsilateral and contralateral sides, sending no significant collaterals within the spinal cord, medulla, or cerebellar nuclei. Strikingly, we find that cervical spinal cord *Atoh1*-lineage neurons form mainly the indirect spino-lateral reticular nucleus and spino-olivary tracts and thoracolumbar *Atoh1*-lineage neurons project locally within the spinal cord, whereas only a few *Atoh1*-lineage neurons form a direct spinocerebellar tract.

Received Aug. 17, 2020; revised Nov. 21, 2021; accepted Nov. 22, 2021.

Author contributions: I.V.P., F.E., C.J.B., P.C.O., O.W.O., M.G., B.M., M.A.L., and H.C.L. performed research; I.V.P., F.E., C.J.B., P.C.O., and H.C.L. analyzed data; I.V.P., F.E., M.G., M.A.L., K.M.D., C.B.G., and H.C.L. edited the paper; C.J.B. and H.C.L. designed research; C.J.B., K.M.D., and C.B.G. contributed unpublished reagents/analytic tools; H.C.L. wrote the first draft of the paper; H.C.L. wrote the paper.

This work was supported by NIH/NIMH R01MH120131, NIH/NIMH R34NS121873, NIH/NCI U54CA268072, NIH/NCI 5P30CA142543, and NIH/NIDDK 1R01DK127589 to K.M.D.; NIH/NHGRI R35HG010719 and NIH/NIGMS R21GM129559 to C.B.G.; and the Rita Allen Foundation, Welch Foundation I-1999-20190330, Kent Waldrep Foundation, and NIH/NINDS R21NS099808 and NIH/NINDS R01NS100741 to H.C.L. We thank Lin Gan for the *Atoh1*$^{Cre/+}$ knock-in mouse; Martyn Goulding for the *Cdx2::FLPo* mouse; Susan Dymecki for the *R26*$^{LSL\text{-}FSF\text{-}TeTx}$ mouse; Mark Behlke and Sarah Jacobi (Integrated DNA Technologies) for providing preproduction megamers; Rebecca Seal for the *Vglut1* ISH probe; Thomas Jessell for the *Gdnf* ISH probe; Heankel Cantu Oliveros and Wei Xu for the Lenti^{FugE}-Cre virus; Christine Ochoa, Jun Chul Kim, and Jungsik Noh for technical assistance; Shari Birnbaum for behavioral assistance; the Neuroscience Microscopy Facility, which is supported by the UT Southwestern Neuroscience Department and the UT Southwestern Peter O'Donnell, Jr. Brain Institute, LifeCanvas Technologies for tissue clearing assistance; and Jane Johnson, Peter Tsai, Ariel Levine, Euiseok Kim, Abigail Person, and the H.C.L. laboratory for helpful discussions and careful reading of the manuscript.

The authors declare no competing financial interests.

Correspondence should be addressed to Helen C. Lai at Helen.Lai@utsouthwestern.edu.

https://doi.org/10.1523/JNEUROSCI.2157-20.2021

Copyright © 2022 the authors

Introduction

Proprioception, the sense of limb and body position, is critical for generating an online state body map (Sherrington, 1906; Tuthill and Azim, 2018). When proprioception is lost, gross trajectories are maintained, but coordinated limb movement is impaired (Gordon et al., 1995; Abelew et al., 2000; Windhorst, 2007; Akay et al., 2014). Muscle and tendon information detected by proprioceptive sensory neurons is integrated by secondary neurons in the spinal cord and relayed to the cerebellum through both direct and indirect spinocerebellar pathways (Oscarsson, 1965; Bosco and Poppele, 2001; Jiang et al., 2015). In this study, we sought to define the precise anatomy of the proprioceptive system through the spinal cord using genetic tools in mice.

The direct spinocerebellar pathway consists of ipsilaterally projecting dorsal and contralaterally projecting ventral spinocerebellar tracts (DSCT and VSCT), deriving from several anatomically and molecularly distinct groups of soma in diverse laminae throughout the spinal cord where they are thought to convey ongoing locomotor activity (Matsushita and Hosoya, 1979; Sengul et al., 2015). A major contributor to the DSCT comes from Clarke's column (CC) neurons, whose soma reside in the medial aspect of the thoracic to upper lumbar spinal cord (Oscarsson, 1965; Baek et al., 2019). While SCT axons terminate as mossy fiber (MF) terminals on granule cells (GCs) in the cerebellum (Arsenio Nunes and Sotelo, 1985; Reeber et al., 2011), the extent to which CC neurons send axon collaterals to areas within the spinal cord, medulla, or cerebellar nuclei (CN) is unclear (Ekerot and Oscarsson, 1976; Matsushita and Gao, 1997; Mogensen et al., 2017; Luo et al., 2018). Such axon collaterals would be important for integration with other ascending or descending pathways (Sillitoe et al., 2012; Beitzel et al., 2017).

Compared with the direct spinocerebellar pathways, less is known about the anatomy of the indirect spino-lateral reticular nucleus (spino-LRt) and spino-olivary (Helweg's tract) pathways. Spino-LRt neurons project ipsilaterally and contralaterally to the LRt in the medulla where they are involved in posture, reaching, and grasping (Alstermark and Ekerot, 2013; Jiang et al., 2015). Spino-olivary neurons reside in lamina V-VII of the spinal cord and project contralaterally to the inferior olive (IO) in the medulla (Oscarsson and Sjolund, 1977a,b; Berkley and Worden, 1978; Swenson and Castro, 1983a,b). Neurons in the IO are thought to be involved in the timing of motor commands, motor learning, and error correction (Sillitoe et al., 2012; White and Sillitoe, 2017).

Developmentally, the basic helix-loop-helix transcription factor-expressing progenitor domains *Atoh1* (atonal homolog 1) and the dorsal *Neurog1* (neurogenin 1) domains are reported to differentiate into neurons of the direct spinocerebellar pathway (Bermingham et al., 2001; Gowan et al., 2001; Sakai et al., 2012). The soma of *Atoh1*-lineage neurons reside medially, laterally, and ventrally to CC neurons, suggesting that CC neurons do not develop from *Atoh1*-lineage neurons, but from an alternate progenitor domain (Yuengert et al., 2015). Based on the location of *Atoh1*-lineage neurons, we previously hypothesized that they make other direct spinocerebellar neurons, such as the lamina V-SCTs or dorsal horn-SCTs (Matsushita and Hosoya, 1979; Edgley and Gallimore, 1988).

In this study, we sought to provide clarity to the development and anatomy of the proprioceptive system using genetic labeling strategies, whole tissue clearing and imaging, and tracing tools of CC and spinal cord *Atoh1*-lineage neurons. We find that CC neurons develop from a *Neurog1*, not *Atoh1*, progenitor population. We also find that, as a population, CC axons do not collateralize considerably to any structures within the spinal cord, medulla, or CN, although they do collateralize extensively within the cerebellar cortex with some axons crossing the midline within the cerebellum. Furthermore, we find that cervical *Atoh1*-lineage neurons make the indirect spino-LRt and spino-olivary tracts rather than the direct lamina V-SCTs or dorsal horn SCTs as originally hypothesized and that thoracolumbar *Atoh1*-lineage neurons project mainly locally within the spinal cord. Together, we provide novel insights into the development and anatomy of spinal cord proprioceptive pathways.

Materials and Methods

Mouse strains

The following mouse strains were used: $Gdnf^{IRES2\text{-}CreERT2}$ (Cebrian et al., 2014) (abbreviated $Gdnf^{CreER}$, JAX #024948), *Neurog1BAC-Cre* (Quinones et al., 2010) (JAX #012859), $Atoh1^{Cre}$ knock-in (Yang et al., 2010), $R26^{LSL\text{-}LacZ}$ (Soriano, 1999) (JAX #003474), $R26^{LSL\text{-}tdTom}$ (Ai14) (JAX #007914) (Madisen et al., 2010), $R26^{LSL\text{-}FSF\text{-}tdTom}$ (Ai65) (JAX #032864) (Madisen et al., 2015), *Cdx2::FLPo* (Bourane et al., 2015), and $R26^{LSL\text{-}FSF\text{-}TeTx}$ (Kim et al., 2009). We generated the $Atoh1^{P2A\text{-}FLPo}$ knock-in mouse using the Easi-CRISPR method (Quadros et al., 2017; Miura et al., 2018). The model design and its initial characterization are described in our recent work (Ogujiofor et al., 2021). All mice were outbred and are thus mixed strains (including C57Bl/6J, C57Bl/6N, and ICR). $Atoh1^{Cre/+}$ knock-in mice crossed to *Cdx2::FLPo* and dual recombinase tdTomato reporter Ai65 mice were screened for "dysregulated" expression as previously reported (Yuengert et al., 2015). Tamoxifen (Sigma) was injected at P7 and/or P8 for the $Gdnf^{CreER}$ line at 0.1 mg/g mouse using 10 mg/ml tamoxifen dissolved in sunflower oil (Sigma) with 10% ethanol. All animal experiments were approved by the Institutional Animal Care and Use Committee at UT Southwestern.

Tissue processing

Mice are age P0 on the day of birth. Mice older than P10 were anesthetized with Avertin (2,2,2-tribromoethanol; 0.025-0.030 ml of 0.04 M Avertin in 2-methyl-2-butanol and distilled water/g mouse) and transcardially perfused, first with 0.012% w/v heparin/PBS and then 4% PFA/PBS. A dorsal or ventral laminectomy exposed the spinal cord to the fixative. Spinal cords were fixed for 2 h and the brains overnight at 4°C. Tissue was washed in PBS for at least 1 d and cryoprotected in 30% sucrose dissolved in deionized water. Tissue was marked with 1% Alcian Blue in 3% acetic acid on one side to keep orientation and were embedded in OCT (Tissue-Tek Optimal Cutting Temperature compound). Tissue was sectioned using a Leica Microsystems CM1950 Cryostat.

Immunohistochemistry (IHC) and confocal imaging

Cryosections (20-40 μm) were blocked with PBS/1%-3% normal goat or donkey serum (Jackson ImmunoResearch Laboratories)/0.3% Triton X-100 (Sigma) for up to 1 h at room temperature and incubated overnight with primary antibody at 4°C. After washing 3 times with PBS, the appropriate secondary antibody (Alexa-488, -567, and/or -647, Invitrogen) was incubated for 1 h at room temperature. Sections were rinsed 3 times in PBS, mounted with Aqua-Poly/Mount (Polysciences), and coverslipped (Thermo Fisher Scientific). The following primary antibodies and dilutions were used: 1:500 rabbit anti-dsRed (Clontech), 1:500 mouse anti-NEUN (Millipore Sigma), 1:500 chicken anti-GFP (Aves), 1:5000 guinea pig anti-VGLUT1 (Millipore Sigma), 1:1000 guinea pig anti-VGLUT2 (Millipore Sigma), 1:100 goat anti-CHAT (Millipore Sigma), 1:200 rabbit anti-PSD-95 (Invitrogen), and 1:1000 rabbit anti-PV27 (Swant). Sections were referenced to the Mouse Brain Atlas (Paxinos and Franklin, 2007) and Christopher Reeves Spinal Cord Atlas (Watson et al., 2009).

Fluorescent images were taken on a Carl Zeiss LSM710 or LSM880 confocal microscope with an optical slice of 0.5-10 μm depending on the objective used (10× air, 20× air, 40× oil, or 63× oil). Images were

pseudo-colored using a magenta/yellow/blue, magenta/green/blue, or magenta/yellow/cyan color scheme using Adobe Photoshop 2021 (Adobe) or Fiji (Schindelin et al., 2012). Images for quantitation of soma size were processed in Fiji. Images were thresholded and the soma manually outlined to obtain the soma area.

ISH

ISH was performed as per standard protocols. Detailed protocol is available on request. Briefly, spinal cord sections (30 μm) were dried at 50°C for 15 min and then fixed in 4% PFA in DEPC-PBS for 20 min at room temperature. The sections were washed in DEPC-PBS for 5 min at room temperature before and after the incubation in RIPA buffer (150 mM NaCl, 1% NP-40, 0.5% Na deoxycholate, 0.1% SDS, 1 mM EDTA, 50 mM Tris, pH 8.0) for 60 min. Next, the sections were postfixed in 4% PFA in DEPC-PBS for 15 min at room temperature. The sections were then washed in DEPC-water followed by acetylation (500 µl of acetic anhydride in 200 ml of 0.1 M RNase-free triethanolamine-HCl at pH 8.0), washed in DEPC-PBS for 5 min, and prehybridized for 2 h at 60°C-62°C. Sections were incubated overnight at 60°C-62°C with 1-2 ng/µl of fresh probe (*Gdnf* or *Vglut1*). A series of low- and high-stringency washes in 2× and 0.2× SSC as well as treatment with RNaseA and RNase T1 were performed. The sections were blocked in 10% inactivated sheep serum for 1 h followed by overnight incubation with 1:1000 anti-digoxygenin antibody (Roche). The sections were washed in PBT and incubated with NBT/BCIP (Roche) staining solution. After the blue precipitate formed, the slides were washed in PBS and coverslipped with Aqua-Poly/Mount (Polysciences) mounting media.

The RNAscope Fluorescent Multiplex Assay (Advanced Cell Diagnostics) was performed according to the manufacturer's instructions using a *Vglut1* probe (ACDBio, 416631), *Vglut2* probe (ACDBio, 319171), or *Gdnf* probe (ACDBio, 421941). All incubation steps were performed in a HybEZ II oven set to 40°C. The slides were then washed with 1× DPBS (Invitrogen, 14190) and incubated with a 2:1 1× DPBS:Protease III for 150 s. Slides were then washed with 1× DPBS 3 times and incubated with the probe(s) for 2 h. The slides were washed 2 times thoroughly using 1× wash buffer (ACDBio, 310091) for 2 min, then incubated with Amp 1-Fl for 30 min. The same process (washing then treatment) was repeated for Amp 2-Fl, Amp 3-Fl, and Amp 4-Fl for 15, 30, and 15 min, respectively. For antibody staining of β-galactosidase, the sections were transferred to a humidified tray and blocked for 30-45 min in 0.25 ml/slide of PBT (PBS with 0.3% Triton) containing 1% goat serum (Jackson ImmunoResearch Laboratories). The sections were incubated with chicken anti-β-galactosidase antibody (Abcam, 1:500) in PBT with 1% goat serum overnight at 4°C. The slides were then washed 3 times in PBS for 10 min and incubated at room temperature for 1 h with goat anti-chicken AlexaFluor-488 (Invitroten, 1:500). Slides were washed 3 times in PBS for 10 min and coverslipped using 2 drops of Aqua-Poly/Mount (Polysciences) as the mounting media.

X-gal staining

Slides with spinal cord sections (30 µm) were incubated in staining solution with 5 mM $K_3Fe(CN)_6$, 5 mM $K_4Fe(CN)_6$, and 1 mg/ml of X-gal (Roche) until precipitate was sufficient to visualize. Sections were moved to PBS, mounted, and coverslipped.

Viral injections

Mice aged P7-P8 were anesthetized using isoflurane (Henry Schein Medical) and prepared for injections into the spinal cord. The back hair was shaved and 70% ethanol and betadine (Avrio Health L.P.) applied. A midline incision was made on the dorsal surface of the spinal cord. AAV9.hSyn.DIO.eGFP.WPRE.hGH was injected into the lower thoracic spinal cord through the intervertebral space of P7 or P8 $Gdnf^{Tom}$ mice (100 nl total in 27.6 nl increments at 1-2 min intervals, Nanoject II, Drummond Scientific; 1.07×10^{13} GC/ml, Penn Vector Core). Lenti^{FugE}-Cre was injected into the cervical or lower thoracic to lumbar area of P7 $Atoh1^{P2A\text{-}FLPo}$;*Ai65* mice (total of 50.6 nl in 27.6 nl increments at 1-2 min intervals). Lenti^{FugE}-Cre was pseudotyped with a fusion glycoprotein enabling efficient retrograde axonal transport (Kato et al., 2014). To generate Lenti^{FugE}-Cre, the *Cre* coding sequence was subcloned into the third-generation HIV-based lentivirus vector under the control of a synapsin promoter (FSW-*Cre*). FSW-*Cre* was cotransfected into HEK293 cells with three packing plasmids (pMDLg/pRRE, pRSV-Rev, and pCAGGS-FuG-E) to generate Lenti^{FugE}-Cre, which was concentrated with ultracentrifugation to 2.0×10^{12} Vg/ml. The incision was closed with surgical glue (Henry Schein Medical). Carprofen (5 mg/kg) was administered daily 3 d after surgery. Spinal cords were harvested ~3 weeks after injection.

Cholera toxin subunit B (CTB) and Fluorogold (FG) injections

$Gdnf^{Tom}$ mice were injected with 1% (w/v) of CTB-488 (left side) and CTB-647 (right side) (Thermo Fisher Scientific). Mice were anesthetized with isoflurane, and the area above and around the cerebellar region was prepared for surgery. A midline incision of 0.75 cm and a craniectomy of ~1 mm × 1 mm were performed. Bilateral injections at four sites were done at (from bregma): rostrocaudal −5.7 and −6.2 mm and at mediolateral ±0.35 mm. At each site, several injections in 32 nl increments were performed every 300 µm along the dorsoventral axis at coordinates: −1.8 and −1.5 mm deep for a total of 320 nl of conjugated CTB. Animals were killed and tissue harvested 5 d after injection.

FG was injected into the vermis of lobules I-V in the cerebella of $Gdnf^{Tom}$, $Atoh1^{Tom}$, or $Atoh1^{Cre}$;*Cdx2::FLPo;Ai65* mice. Mice (1-2 months old) were injected with 4% (w/v) FG solution in saline (Fluorochrome). Mice were anesthetized with isoflurane, and the area above and around the cerebellar region was prepared for surgery. A midline incision of ~0.75 cm and a craniectomy of ~1 mm wide by 1.5 mm long was performed. Bilateral injections at six sites were done at (from bregma): rostrocaudal −5.6 to −5.5, −5.9, and −6.25 to −6.3 mm and at mediolateral ±0.2 to 0.4 mm. The maximum depth at each rostrocaudal site was −2.0, −2.4, and −1.5 mm, respectively. Multiple injections were done at each site in 32 or 50.6 nl increments every 300 µm along the dorsoventral axis for a total of 270-720 nl of FG on each side. Animals were killed and tissue harvested 7 d after injection.

For FG injections targeting the LRt and IO, $Atoh1^{Tom}$ mice (7-9 weeks old) were anesthetized with isoflurane, and the area above and behind the occipital region prepared for surgery. A midline incision of ~1 cm was made. Neck muscles were detached from the occipital bone and retracted laterally to expose the foramen magnum. A needle with a rostroventral inclination of 47° was used to advance through the foramen magnum into the brainstem ~3.7 mm from dura; 32.2 nl of 1%-2% (w/v) FG solution was injected 4-5 times 25 µm apart while retracting the pipette with an interval of 30 s between injections for a total of 128.8-161 nl of FG. Unilateral injections were done at the following coordinates measured from the most ventral aspect of the occipital crest: rostrocaudal −0.4 mm, and mediolateral ±0.75 mm. After the last injection, the needle was left in place for 3 min and then slowly extracted from the brainstem. Animals were killed and tissue was harvested 7 d after injection.

Whole-tissue imaging

Mouse hindbrain and spinal cords were processed following the SHIELD protocol (Park et al., 2018). Tissues were cleared with SmartClear II Pro (LifeCanvas Technologies) for several days, mounted in a gel of 0.9% agarose in EasyIndex (LifeCanvas Technologies), and then incubated in EasyIndex for refractive index matching. Tissues were imaged at 3.6× using a SmartSPIM light sheet microscope (LifeCanvas Technologies). Spinal cords and hindbrains of 3 mice marking CC were used for quantitation of the MF/cell body ratio: 1 $Gdnf^{Tom}$ mouse (female, P23) and 2 $Gdnf^{CreER}$;*Cdx::FLPo;Ai65* mice (1 male, 1 female, P28). Mice were imaged with 1.8 µm × 1.8 µm × 2 µm sampling (*X*, *Y*, and *Z*, respectively). The total number of 2 µm image slices for each sample was as follows: spinal cord (1500, 3300, 2400 slices) and hindbrain (2700, 3000, 3300 slices) for the $Gdnf^{Tom}$, $Gdnf^{CreER}$;*Cdx::FLPo;Ai65* male, $Gdnf^{CreER}$;*Cdx::FLPo;Ai65* female mouse, respectively. One $Atoh1^{Cre}$;*Cdx::FLPo;Ai65* mouse spinal cord and hindbrain were cleared (male, P30). The hindbrain was imaged as described above (4800 slices). The spinal cord was imaged with a 15× objective with 0.41 µm × 0.41 µm × 2 µm sampling (900 slices). All hindbrain and spinal cord samples were cut to <2.2 cm

to fit in the imaging chamber. Movies were made using arivis Vision4D 2.12.6. Maximum intensity projections (MIPs) were processed using Fiji (Schindelin et al., 2012).

Behavioral test: rotarod

Rotarod was performed at 8-13 weeks of age. Tester was blind to genotype. Mice were acclimated to the testing room for 0.5-1 h on day of testing. All mice were genotyped for appropriate alleles using previously published protocols for *Atoh1*^{Cre}, *Cdx::FLPo*, and *R26*$^{LSL\text{-}FSF\text{-}TeTx}$ (Kim et al., 2009; Yang et al., 2010; Bourane et al., 2015). Mice were placed on an accelerating rotarod (IITC Life Science Series 8) from 4-40 RPM over 5 min. Four trials were performed each day for 2 d with at least a 15 min wait time between trials. The genotype control group consisted of *Atoh1*^{Cre}*;TeTx* het ($n = 11$, 8 F:3 M), *Cdx2::FLPo;TeTx* het ($n = 20$, 9 F:11 M), and TeTx het ($n = 5$, 3 F:2 M) for a total of $n = 36$ control mice compared with *Atoh1*^{Cre}*;Cdx2::FLPo;TeTx* het ($n = 22$, 10 F:12 M) test animals.

Assessment of GFP-tetanus toxin (GFP-TeTx) expression

We made several attempts to assess GFP-TeTx expression in *Atoh1*^{Cre}*; Cdx2::FLPo;R26*$^{LSL\text{-}FSF\text{-}TeTx}$ mice at the mRNA or protein level. In all cases, GFP-positive control animals gave the appropriate positive signal, but no GFP-TeTx was detected. We have reason to believe, though, that the GFP-TeTx is below the limit of detection in these animals and may be inefficiently expressed in certain cell types because we found that GFP-TeTx is expressed and functional in an *Atoh1*^{Cre}*;Cdx2::FLPo; R26*$^{LSL\text{-}FSF\text{-}TeTx}$ mouse with dysregulated *Atoh1*^{Cre} expression. In this mouse, the dysregulated CRE combined with FLPo expression allows for GFP-TeTx expression in many caudal cell types. Thus, we can detect GFP and TeTx mRNA expression by RNAscope in the lumbar spinal cord of this mouse. Correspondingly, this mouse was unable to perform on the rotarod assay indicating the GFP-TeTx is functional (unpublished observations). This mouse was not included in our cohort. Together, we find that the GFP-TeTx is likely very sparsely expressed in our mice, leading to the inconclusive phenotype in the rotarod assay. We describe our attempts at detecting GFP-TeTx expression here for reference.

IHC. IHC using chick anti-GFP was amplified with a fluorescent secondary antibody and visualized by confocal microscopy as described above. We also tried IHC to Synaptobrevin 2 (VAMP2), the target of GFP-TeTx, using mouse anti-Synaptobrevin 2 antibody (Synaptic Systems, 104211) and saw no change in areas where GFP-TeTx should be expressed compared with controls.

DAB staining. Cryosections were processed with the VECTASTAIN Elite ABC-HRP kit (rabbit IgG) (Vector Laboratories, PK6101) following manufacturer's instructions. Briefly, the sections were exposed to quenching buffer (Hydrogen Peroxide blocking reagent, Abcam, ab64218) and incubated with normal goat serum blocking solution. The sections were then incubated with rabbit anti-GFP antibody (either Invitrogen A-6455 at 1:500 or 1:40,000 dilution or Invitrogen A-11 122 at 1:500 dilution) for 72 h and with a biotinylated goat anti-rabbit IgG secondary antibody followed by incubation in avidin/biotinylated HRP reagent. The sections were then incubated in the DAB substrate solution (3,3′ diaminobenzidine tetrahydrochloride [Sigma] in Tris-HCl buffered saline [TBS] and H_2O_2). Sections were dehydrated and mounted with DPX mounting media (Sigma).

Gfp *and* TeTx *ISH.* The sequence and plasmid to generate *Gfp* and *TeTx* ISH probes were kindly provided by Jun Chul Kim. A 693 bp probe to *Gfp* was generated using the following primers: 5′-GAGAG TGATCCCGGCGGCGG-3′ and 5′-GTGAGCAAGGGCGAGGAGC TG-3′. An 858 bp probe to *TeTx* was generated using the following primers: 5′-GATATCGATGGAGATCAGG-3′ and 5′-CCGATCACC ATCAACAACTTC-3′. *In situ* plasmids are available on request. ISH performed as described above.

Gfp *and* TeTx *RNAscope.* RNAscope using EGFP (ACDBio, 400281-C2) and Syntetanus (ACDBio, 537461-C2) probes were performed as described above.

Western to GFP. Western was performed as per standard protocols. Briefly, lower thoracic to upper lumbar spinal cords were homogenized and lysed in RIPA buffer (Sigma-Aldrich) with Halt Protease/Phosphatase Inhibitor Cocktail (Thermo Fisher Scientific) and 1 mM EDTA (Sigma). Lysates were centrifuged to obtain the supernatant. Samples were diluted to a final concentration of 1× Laemmli buffer (Bio-Rad) and 50 mM DTT (Sigma). Proteins were separated by gel electrophoresis and transferred to an Immobilon PVDF membrane (Millipore) and blocked in 5% nonfat dry milk in TBS containing 0.1% Tween-20. Membranes were probed with the following primary antibodies: rabbit anti-GFP polyclonal (Invitrogen, A-6455, 1:7500 and A-11122, 1:2000), mouse anti-GFP monoclonal (Invitrogen, MA5-15256, 1:1000 and A-11120, 1:5000), and rabbit anti-β-actin (Cell Signaling, 4967, 1:1000) for loading control. Goat anti-rabbit HRP (Cell Signaling Technology, 7074, 1:2000) and goat anti-mouse HRP (Invitrogen, G-21 040, 1:10,000) secondary antibodies were used. Bands were visualized by enhanced chemiluminescence according to the manufacturer's instructions (Thermo Fisher Scientific) and scanned using the GelDoc Go Gel Imaging System (Bio-Rad).

Experimental design and statistical tests

The MF to cell body ratio (see Fig. 3*K*) was counted from three cleared spinal cords and hindbrains. Cells bodies in the spinal cord and MFs in the cerebellar cortex were counted from 100 µm MIP images of cleared tissue. The ratio calculated is an estimate given that it is impossible to accurately count all the cell bodies and MF terminals, and there are many opportunities for overcounting or undercounting. For example, although cell bodies and MFs were counted only when they could be discretely identified, some MF terminals might appear as two MF terminals, when they indeed come from the same MF. As an example of undercounting, cell bodies and MFs may overlap in the z axis of the 100 µm MIP and may be counted as one instead of several. Together, cell bodies and MFs were counted to get an estimate rather than an exact count of the MF/cell body ratio.

For the mapping of thoracolumbar CC MF terminals in the cerebellum (see Fig. 4*H-H′′′,J-J′′′,L-L′′′,N,P,R*), confocal images of 30 µm cryosections were analyzed in Fiji using the ROI Manager to label individual MF terminals and the SlideSet PlugIn to export the ROIs as a .svg file (Schindelin et al., 2012; Nanes, 2015). These mapped MF terminals were then overlaid on a traced drawing of the confocal image in Adobe Illustrator 2021.

All data and graphs were processed in Microsoft Excel 2015 and GraphPad Prism 9. Details of the number of sections counted and sex of the mice are given in Results. Data are mean ± SEM throughout the manuscript. Statistical tests used are detailed in Results and/or figure legends.

Results

CC is the major direct spinocerebellar pathway in mice

To assess the spinocerebellar system in mice, we identified genetic tools that reproducibly label spinal cord neurons and evaluated their contribution to the spinocerebellar system using a combination of retrograde and anterograde tracing. Previously, we found that the *Atoh1*-expressing progenitor population that makes dorsal interneuron 1 (dI1) neurons, although implicated in making spinocerebellar neurons developmentally (Bermingham et al., 2001; Gowan et al., 2001; Sakai et al., 2012), rarely made CC neurons, which are the major source of the DSCT (Fig. 1*A*; note the absence of TOM$^+$ cells in the CC area of *Atoh1*-lineage traced neurons, *Atoh1*^{Cre}*;R26*$^{LSL\text{-}tdTom}$ (Ai14), abbreviated *Atoh1*^{Tom}) (Madisen et al., 2010; Yang et al., 2010; Yuengert et al., 2015). Therefore, we sought to identify the progenitor population that gives rise to CC neurons. Evidence from spinal cord development suggested that the neighboring *Neurog1*-expressing progenitor population that makes dI2 neurons also project to the cerebellum (Avraham et al., 2009; Sakai et al., 2012). Because there are no uniquely specific molecular markers for the dI2 population, we traced the lineage of the entire *Neurog1* population, which includes dI2 neurons and ventral domains, using a transgenic

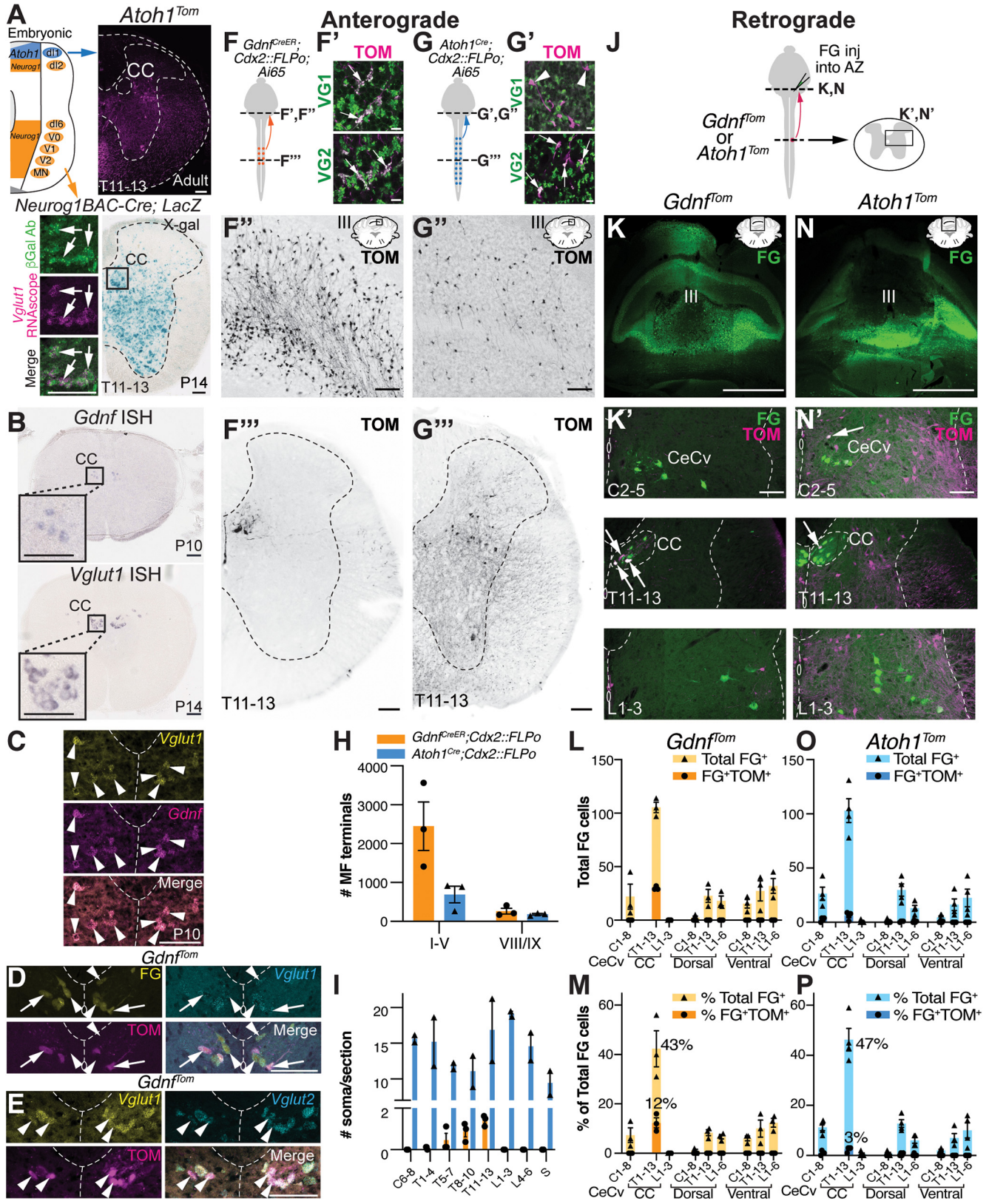

Figure 1. CC is the major direct spinocerebellar pathway in mice. ***A***, Lineage tracing of *Neurog1*-expressing progenitors (*Neurog1BAC-Cre* crossed to *R26*$^{LSL\text{-}LacZ}$) in the neural tube identifies large CC neurons in the thoracic spinal cord (box in X-gal stain). β-Gal expressing cells (green) colocalize with the CC marker, *Vglut1* mRNA (magenta, arrows). *Atoh1*-lineage neurons (*Atoh1*^{Tom}) reside lateral and ventral to CC. ***B***, CC is marked by expression of *Gdnf* and *Vglut1* mRNA. ***C***, *Gdnf* and *Vglut1* mRNA colocalize in CC neurons at P10 by RNAscope (arrowheads). ***D***, CC neurons retrogradely labeled with FG colocalize with *Vglut1* mRNA (FG$^+$*Vglut1*$^+$, arrowheads). A subset of CC neurons are labeled with *Gdnf*^{Tom} (FG$^+$TOM$^+$*Vglut1*$^+$, arrows). ***E***, CC neurons marked by *Gdnf*^{Tom} express both *Vglut1* and *Vglut2* mRNA (arrowheads). ***F-I***, Comparison of MF terminals in the cerebellum of CC and caudal *Atoh1*-lineage neurons. Diagram of CC and caudal *Atoh1*-lineage neurons labeled with tdTomato (TOM) (***F***,***G***). MF terminals in the cerebellum of CC neurons are VGLUT1$^+$ (VG1) and VGLUT2$^+$ (VG2) (***F'***, arrows). MF terminals of caudal *Atoh1*-lineage neurons are VG2$^+$ (***G'***, arrows), but VG1$^-$ (***G'***, arrowheads). Fewer MF terminals are seen in the cerebellum from caudal *Atoh1*-lineage neurons (***G''***) than CC neurons (***F''***).

Neurog1BAC-Cre strain crossed to a $R26^{LSL\text{-}LacZ}$ reporter mouse (Fig. 1*A*) (Soriano, 1999; Quinones et al., 2010). Large CC cells residing in the medial thoracic spinal cord colocalize with vesicular glutamate transporter 1 (*Vglut1*) mRNA, a marker for CC (Fig. 1*A*,*B*) (Llewellyn-Smith et al., 2007; Malet et al., 2013; Yuengert et al., 2015). Therefore, CC neurons come from a *Neurog1*-lineage (dI2 or ventral lineages), but not the *Atoh1*-lineage.

Next, we further characterized molecular tools that label CC neurons. As previously described, CC neurons are marked by glial-derived nerve growth factor (*Gdnf*) and *Vglut1* mRNA (Fig. 1*B*) (Llewellyn-Smith et al., 2007; Hantman and Jessell, 2010; Malet et al., 2013). We found that *Gdnf* is transiently expressed from E18.5 to P10 (data not shown) and that *Gdnf* and *Vglut1* mRNA completely overlap at P10 (Fig. 1*C*, arrowheads). Furthermore, CC neurons that are retrogradely labeled with FG injected into the anterior zone (AZ, lobules I-V) of the cerebellum, colocalized with *Vglut1* mRNA (Fig. 1*D*, arrowheads). A subset of CC neurons is labeled using a $Gdnf^{IRES2\text{-}CreERT2/+}$ mouse line crossed to a CRE-dependent tdTomato reporter (Ai14, abbreviated $Gdnf^{Tom}$ from here on; Fig. 1*D*, arrows) (Hantman and Jessell, 2010; Cebrian et al., 2014). Last, we found that CC neurons also express vesicular glutamate transporter 2 (*Vglut2*) (Fig. 1*E*, arrowheads). We used the $Gdnf^{IRES2\text{-}CreERT2/+}$ mouse line (abbreviated $Gdnf^{CreER}$ from here on) for the remainder of the study because of its specific labeling of CC neurons.

To understand the relationship of the direct spinocerebellar system to our two CRE mouse lines ($Gdnf^{CreER}$ and $Atoh1^{Cre}$), we used both anterograde (Fig. 1*F–I*) and retrograde (Fig. 1*J–P*) tracing strategies to and from the cerebellum. To identify ascending projections from the spinal cord, we used an intersectional strategy to restrict labeling of neurons to regions caudal of cervical 4 (C4; *Cdx2::FLPo*) (Bourane et al., 2015). As expected, we found that CC neurons ($Gdnf^{CreER}$; *Cdx2::FLPo; Ai65*) terminate as MFs in the AZ of the cerebellum and express $VGLUT1^+$ (VG1) and $VGLUT2^+$ (VG2) presynaptic markers (Fig. 1*F–F‴*). However, labeling of caudal *Atoh1*-lineage neurons ($Atoh1^{Cre}$; *Cdx2::FLPo*; *Ai65*) had very few MF terminals in the AZ, although they were $VG1^-$ and $VG2^+$, consistent with a non-Clarke's spinocerebellar population and a previous report that spinocerebellar neurons are mainly $VG2^+$ with some $VG1^+$ MF terminals (Gebre et al., 2012; Yuengert et al., 2015) (Fig. 1*G-G‴*; quantitated in Fig. 1*H*, in the AZ, 2447 ± 624 $Gdnf^{CreER}$; *Cdx2::FLPo; Ai65* ($n = 3$, 2 females (F):1 male (M)) vs 690 ± 213 $Atoh1^{Cre}$; *Cdx2::FLPo*; *Ai65* ($n = 3$, 1 F:2 M), *t* test $p = 0.056$, three comparable sections/*n*; MF terminals in lobules VIII/IXa are similar, 262 ± 75 $Gdnf^{CreER}$; *Cdx2::FLPo; Ai65* vs 182 ± 21 $Atoh1^{Cre}$; *Cdx2::FLPo*; *Ai65*, 1 comparable section/*n*; ages P27-P67). The difference in MF terminals is striking given that *Atoh1*-lineage neurons have many more soma per section throughout the rostral-caudal axis compared with CC neurons (Fig. 1*I*, $Gdnf^{CreER}$; *Cdx2::FLPo; Ai65*, $n = 3$, 2 F:1 M, four sections counted per region per *n*; $Atoh1^{Cre}$; *Cdx2::FLPo*; *Ai65*, $n = 2$, 1 F:1 M, 3 or 4 sections counted per region per *n*), suggesting there are many more MF terminals per CC soma in the spinal cord compared with caudal *Atoh1*-lineage neurons.

Consistent with our anterograde tracing findings, we found that retrograde labeling of spinocerebellar neurons colocalized with CC neurons, but few *Atoh1*-lineage neurons (Fig. 1*J–P*). FG was injected into the cerebella of $Gdnf^{Tom}$ or $Atoh1^{Tom}$ mouse strains targeting the AZ where spinocerebellar neurons are known to project (Fig. 1*J*,*K*,*N*) (Arsenio Nunes and Sotelo, 1985; Bosco and Poppele, 2001; Reeber et al., 2011). Overall, FG retrograde tracing from all injections was similar with 261 ± 39 total FG^+ cells in injections of $Gdnf^{Tom}$ ($n = 3$, 1 F:2 M, ages P38-P40, counts from 5 sections per spinal cord region per *n*) and 228 ± 32 total FG^+ cells in injections of $Atoh1^{Tom}$ ($n = 4$, 3 F:1 M, ages P39-P40, counts from 5 sections per spinal cord region per *n*) (Fig. 1*L*,*O* shows total FG cells in each spinal cord region). Overall, CC is the most abundantly labeled spinocerebellar projection making up 43%-47% of all retrogradely labeled FG neurons in the spinal cord (Fig. 1*M*,*P*). The next most abundant areas of spinocerebellar neurons along the rostral-caudal axis are those in the central cervical (CeCv) nucleus (Cummings and Petras, 1977; Wiksten, 1987; Popova et al., 1995) and cells dorsal or ventral of the central canal in the thoracolumbar areas (Fig. 1*K′*,*N′*, top and bottom panels; Fig. 1*L*,*M*,*O*,*P*), which correspond to LV-SCT, LVII-SCT, LVIII-SCT, and spinal border cells (Baek et al., 2019). Notably, spinocerebellar neurons in the CeCv and thoracolumbar areas (excluding CC) are rarely colabeled with $Gdnf^{Tom}$ or $Atoh1^{Tom}$ neurons (Fig. 1*L*,*M*,*O*,*P*), indicating that genetic labels for these spinocerebellar neurons and their developmental origins have yet to be determined. $Gdnf^{Tom}$ makes up 12 ± 2% of the FG^+ CC neurons out of all FG^+ neurons in the spinal cord and therefore labels ~29 ± 1% of CC neurons. The remaining ~70% of unlabeled CC neurons in the $Gdnf^{Tom}$ line could be because of the restricted time point at which tamoxifen was injected (P7-P8), incomplete CRE recombination, or represent a unique subset of CC neurons. $Atoh1^{Tom}$ makes up 3 ± 1% of the FG^+ CC neurons out of all FG^+ neurons in the spinal cord and therefore labels ~6 ± 1% of CC neurons, consistent with our previous findings that *Atoh1*-lineage neurons make up very few CC neurons (Yuengert et al., 2015). Significantly, only 4 ± 1% of all spinocerebellar (FG^+) neurons projecting to the AZ in the entire spinal cord are *Atoh1*-lineage neurons (FG^+TOM^+). Together, our data suggest that CC makes up a majority of spinocerebellar neurons projecting directly to the AZ, while *Atoh1*-lineage neurons make up very few direct spinocerebellar neurons. Using our genetic tools, we then proceeded to determine the precise anatomy of both CC and *Atoh1*-lineage projections.

Anatomical trajectories of CC neurons

We used the $Gdnf^{Tom}$ line to meticulously trace axonal trajectories of CC neurons to the cerebellum. We found that the axons

←

Representative thoracic sections of CC and caudal *Atoh1*-lineage neurons (***F‴***,***G‴***). Quantitation of MF terminals in the vermis of lobules I-V and VIII/IX (***H***) and of the number of soma in the spinal cord (***I***) for CC and caudal *Atoh1*-lineage neurons. ***J-P***, Comparison of spinocerebellar neurons retrogradely labeled with FG in mice with CC ($Gdnf^{Tom}$) or *Atoh1*-lineage ($Atoh1^{Tom}$) neurons labeled with tdTomato (TOM). Diagram of FG cerebellar injections into the AZ (lobules I-V) of either $Gdnf^{Tom}$ or $Atoh1^{Tom}$ mice to retrogradely label direct spinocerebellar projections (***J***). FG injection in the cerebellum (***K***,***N***, green) retrogradely labels CeCv cells in the cervical spinal cord (***K′***,***N′***, top panels), CC in the thoracic spinal cord (***K′***,***N′***, middle panels), and neurons in other areas of the spinal cord (***K′***,***N′***, bottom panels). Retrogradely labeled CC neurons (green) colocalize with the genetic label for CC ($Gdnf^{Tom}$) (***K′***, middle panel, FG^+TOM^+, arrows), but only occasionally colocalize with *Atoh1*-lineage ($Atoh1^{Tom}$) neurons in CeCv or CC (***N′***, arrows). Quantitation of the total number of FG^+ cells (***L***,***O***) and percentage of total FG^+ cells (***M***,***P***) in a given region of the spinal cord (light orange or light blue) with the total number or percentage of FG^+TOM^+ cells superimposed (dark orange or dark blue) for CC and caudal *Atoh1*-lineage neurons is shown. Spinal cords were divided into cervical (C), thoracic (T), and lumbar (L) areas. The CeCv and CC areas are delineated separately with all other cells categorized based on their C, T, or L location and whether they were dorsal or ventral to the central canal. Spinocerebellar cells dorsal or ventral to the central canal are generally not labeled by $Gdnf^{Tom}$ or $Atoh1^{Tom}$ (***L***,***M***,***O***,***P***). P, Postnatal. Scale bars: ***K***, ***N***, 1 mm; ***A-E***, ***F′***, ***F‴***, ***G′***, ***G‴***, ***K′***, ***N′***, 100 μm; ***F′***, ***G′***, 10 μm. Results in graphs are mean ± SEM.

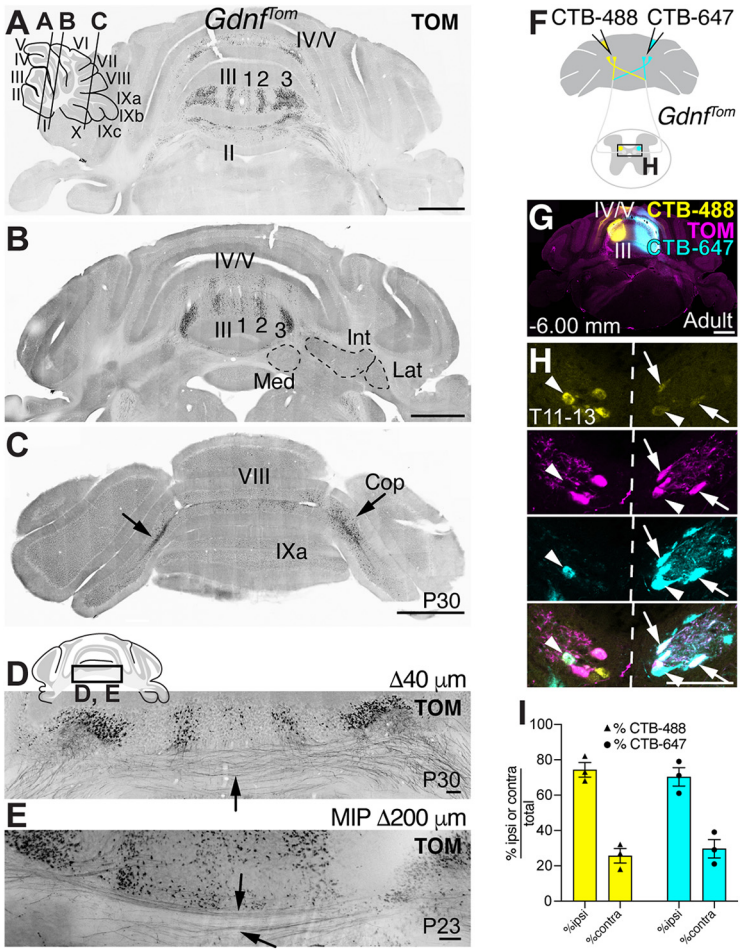

Figure 2. CC MFs terminate ipsilaterally and contralaterally in the cerebellar vermis. ***A-C***, Coronal sections from *Gdnf*^{Tom} mice reveal CC MF terminals (TOM$^+$) in lobules II-V, VIII, IXa, and the copula (***C***, Cop, arrows). Parasagittal stripes (1, 2, 3) in lobule III are apparent. ***D***, ***E***, Some CC axons (TOM$^+$) cross the midline (***D***, arrow, cryosection, and ***E***, arrows, cleared sample, 200 μm MIP). ***F***, Diagram of dual CTB-488 and CTB-647 injections in *Gdnf*^{Tom} mice. ***G***, Coronal section showing the injection site of CTB-488 and CTB-647. ***H***, CC neurons are colabeled with the fluorescent CTB injected on the ipsilateral side as well as the fluorescent CTB injected on the contralateral side (CTB-488$^+$CTB-647$^+$, arrows and arrowheads,). Some cells also colocalize with the *Gdnf*^{Tom} genetic label for CC (TOM$^+$CTB-488$^+$CTB-647$^+$, arrows) and some do not (TOM$^-$CTB-488$^+$CTB-647$^+$, arrowheads). ***I***, Quantitation of the percentage of ipsilaterally or contralaterally labeled CTB$^+$ cells out of all CTB$^+$ cells labeled in the spinal cord with a particular CTB fluorophore (mean ± SEM). Med, Medial; Int, interpositus; Lat, lateral. Scale bars: ***A***, ***B***, ***C***, ***G***, 1 mm; ***D***, ***E***, ***H***, 100 μm.

cross within the cerebellum and terminate almost exclusively as MFs on GCs. We found that CC MF terminals in the cerebellum terminate in the vermis of lobules II-V, VIII, IXa, and the copula pyramidis (Cop) (Fig. 2*A*–*C*), consistent with the termination locations of spinocerebellar neurons from previous pan-anterograde tracing studies (Arsenio Nunes and Sotelo, 1985; Bosco and Poppele, 2001; Apps and Hawkes, 2009; Reeber et al., 2011). In addition, the three parasagittal stripes in lobule III on both sides of the midline closely matched those found in anterograde tracing studies from the thoracic and lumbar spinal cord (Fig. 2*A*,*B*) (Ji and Hawkes, 1994; Reeber et al., 2011). However, while CC axons are known to travel rostrally ipsilaterally in the lateral funiculus of the spinal cord (Oscarsson, 1965) (Movie 1), we found that several axons appeared to cross the midline within the cerebellum (Fig. 2*D*,*E*), suggesting that CC axons terminate both ipsilaterally and contralaterally in the cerebellar cortex, which has been seen in single-cell reconstructions (Luo et al., 2018). To test whether CC axons from a given CC cell terminate on both sides of the cerebellum, we injected two different CTB-conjugated fluorophores (CTB-488 and CTB-647) into the left and right sides of the cerebellum (Fig. 2*F*,*G*). We found retrogradely labeled cells in CC of the spinal cord that took up both tracers (Fig. 2*H*, arrows and arrowheads), some of which were colabeled with *Gdnf*^{Tom} (Fig. 2*H*, arrows); ~30% of the terminals from CC neurons that innervate the injection area are from the contralateral side (% ipsi and contra CTB-488/total CTB-488: 74 ± 4% and 26 ± 4%, respectively; % ipsi and contra CTB-647/total CTB-647: 70 ± 5% and 30 ± 5%, respectively, $n = 3$, 2 F:1 M, 8 sections/n, age P65-P95). This could mean that only 30% of CC neurons cross or that all of them cross, but only some CC neurons have enough terminations on the contralateral side to allow for sufficient CTB uptake. Therefore, CC neurons project ipsilaterally within the spinal cord but send collaterals to both ipsilateral and contralateral sides within the cerebellum.

Strikingly, we found that CC axons do not make significant axon collaterals within the spinal cord, medulla, or to the cerebellar nuclei, a feature typical of other MF tracts, but has been ambiguous for the spinocerebellar system (Fig. 3*A*–*H*′) (Matsushita and Ikeda, 1970; Matsushita and Gao, 1997; Mogensen et al., 2017). In three separate samples, we found no axon terminations in the medial (Med), interpositus (Int), or lateral (Lat) CN. Areas near the CN that had TOM$^+$ signal came from axons of passage and not synaptic terminations (TOM$^+$ axons are VG1$^-$ or VG2$^-$; Fig. 3*A*′,*A*″,*D*′,*D*″). Furthermore, we find no seeming axon collaterals within the spinal cord (Movie 1), nor do we find significant synaptic terminations in the LRt or nucleus X, as was reported previously for some CC neurons (Fig. 3*G*–*H*′) (Luo et al., 2018). Some synaptic terminals can be seen in the LRt

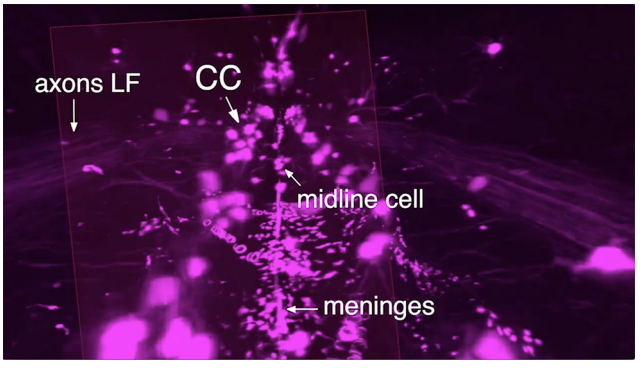

Movie 1. *Gdnf*^{Tom} cleared spinal cord. CC cell bodies line the thoracic midline with axons projecting to the LF and then turning rostrally. The *Gdnf*^{Tom} mouse line also labels smooth muscle cells lining blood vessels within the spinal cord and along the meninges. TOM$^+$ cells along the central canal are also labeled. [View online]

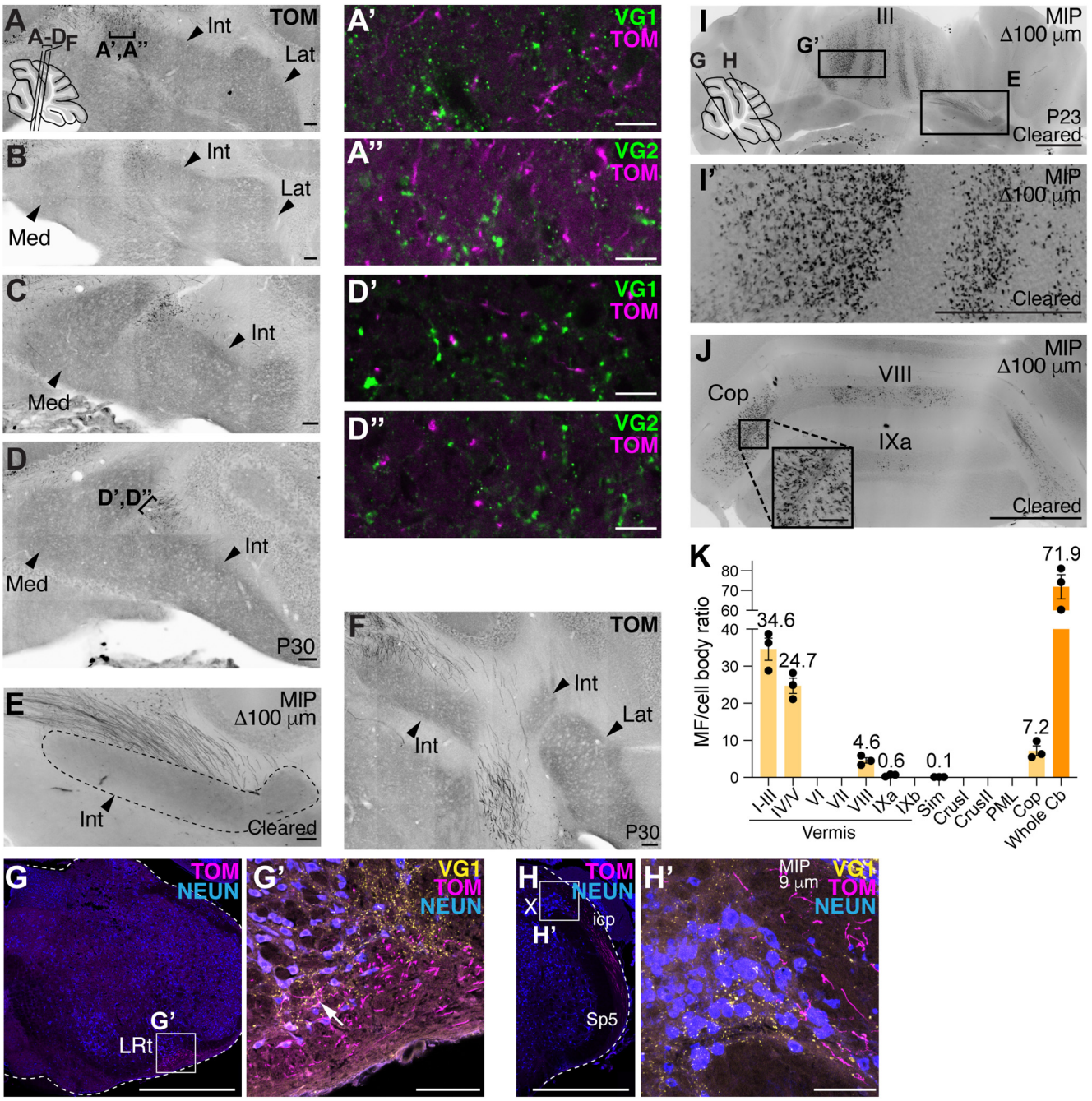

Figure 3. CC neurons do not collateralize to the medulla or CN but arborize extensively in the cerebellar cortex. ***A-D′′***, Almost no CC $Gdnf^{Tom}$ axons enter or are near the CN (arrowheads, Med, Int, Lat). ***A-D***, Successive sections 160 μm apart. Areas of TOM^+ signal near CN do not colocalize with presynaptic markers VG1 (***A′***,***D′***) or VG2 (***A′′***,***D′′***), indicating that these are axons of passage and not presynaptic terminals. ***E***, CC axons (TOM^+) avoid the CN in another $Gdnf^{Tom}$ mouse whose cerebellum was cleared (100 μm MIP). ***F***, CC axons (TOM^+) avoid the CN (40 μm cryosection) in another example $Gdnf^{Tom}$ mouse. Images are from 2 female (***A-E***) and 1 male (***F***) mice ($n = 3$). ***G-H′***, Only a few axonal terminations are seen in the LRt (***G-G′***, arrow) and none in nucleus X (***H-H′***) (verified in $n = 3$ mice, representative sections shown). ***I-K***, Example images of 100 μm MIP from a $Gdnf^{Tom}$ cleared cerebellum. CC MF terminals (TOM^+) are seen in II-V, VIII, IXa, and Cop. ***K***, Quantification of the MF/cell body ratio ($n = 3$ mice: 1 $Gdnf^{Tom}$ and 2 $Gdnf^{CreER}$; *Cdx2::FLPo; Ai65* mice). Overall, the whole cerebellum (Cb) has an estimated 71.9 MF terminals per CC cell body in the spinal cord (orange bar, mean ± SEM). Most MF terminals from CC cells terminate in I-III, IV/V, VIII/IXa, and Cop (light orange bars). Med, Medial; Int, interpositus; Lat, lateral; LRt, lateral reticular nucleus; X, nucleus X; icp, inferior cerebellar peduncle; Sp5, spinal trigeminal tract. Scale bars: ***G***, ***H***, ***I***, ***I′***, ***J***, 1 mm; ***A-F***, ***G′***, ***H′***, ***J***, inset, 100 μm; ***A′-A′′***, ***D′-D′′***, 10 μm.

(Fig. 3*G′*, arrow), but the axons mainly appear to be coursing by the LRt. In summary, our genetic studies of CC neurons show that these glutamatergic neurons terminate bilaterally in the cerebellar vermis but do not make significant axon collaterals to the spinal cord, medulla, or cerebellar nuclei.

Diversification of proprioceptive information through CC neurons

To obtain a three-dimensional view of CC trajectories, we chemically cleared the spinal cords and hindbrains of $Gdnf^{Tom}$ and $Gdnf^{CreER}$;*Cdx2::FLPo*; *Ai65* mice (Movies 1 and 2). Because *Gdnf* is also expressed in smooth and skeletal muscle (Trupp et al., 1995;

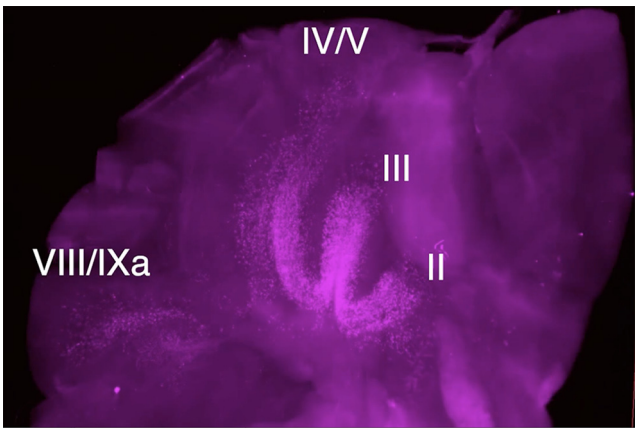

Movie 2. *Gdnf^{CreER}; Cdx2::FLPo; Ai65* cleared hindbrain. CC axons terminate as MFs in the vermis of lobules I-V, VIII, IXa, and copula (cop). Axons from the spinal cord project directly to the cerebellar cortex avoiding the medulla and cerebellar nuclei. [View online]

Suzuki et al., 1998; Rodrigues et al., 2011), they are prominently labeled with TOM in these samples. In the spinal cord (Movie 1), the CC soma can be seen straddling the midline, while their axons extend to the lateral funiculus (LF) where they make a 90° turn heading rostrally to the cerebellum. Axons in the inferior cerebellar peduncle are seen traveling directly to the cerebellum (Movie 2).

A feature that was readily apparent from the cleared specimens was the sheer number of MF terminals in the cerebellum indicating an immense diversification of proprioceptive information coming from CC axons (Fig. 3*I–K*). We counted the number of MF terminals per CC soma in the cerebella and spinal cords of the three cleared samples. From these counts, we estimate that there are 71.9 ± 6.1 MF terminals in the entire cerebellum for each CC soma (Fig. 3*K*, orange bar). The MFs terminate largely in vermis I-III (34.6 ± 3.0 MF/soma ratio), IV/V (24.7 ± 2.1), VIII (4.6 ± 0.7), IXa (0.6 ± 0.2), and the copula (7.2 ± 1.3) ($n = 3$, 2F:1 M, ages P23-P28), consistent with the distribution seen in cryosections (Fig. 2*A–C*). The large ratio of MFs to CC soma suggests that CC information is widely distributed within the cerebellum. Furthermore, the proprioceptive information coming into CC neurons require surprisingly few CC neurons to relay that information to the cerebellum. We counted a range of 486-816 CC neurons in the three spinal cords, which represents ~29% or less of all CC neurons labeled in the *Gdnf^{Tom}* and *Gdnf^{CreER};Cdx2::FLPo*; *Ai65* mouse models for an estimated 1620-2720 CC neurons in the mouse spinal cord. This suggests that most of the mouse proprioceptive direct spinocerebellar system comes from ~2000 neurons.

Next, we wanted to test whether CC neurons from a restricted area of the spinal cord terminate in clustered or diverse locations in the cerebellum. If a given CC neuron sends MFs terminals to one discrete localized area of the cerebellum, this would suggest that proprioceptive information exists as a traditional homunculus in the cerebellum. However, if a given CC neuron sends MF terminals to multiple areas of the cerebellar cortex, this would provide an anatomic substrate for the fractured somatotopic map that has been detected electrophysiologically (Shambes et al., 1978), where body parts are represented in discontinuous patches across the cerebellum (Manni and Petrosini, 2004; Apps and Hawkes, 2009). To label CC neurons specifically in the thoracolumbar area, we injected AAV9-Syn-DIO-EGFP into *Gdnf^{Tom}* mice (Fig. 4*A*). Our injections labeled CC neurons on both sides of the spinal cord (Fig. 4*B,B′*, arrows) and largely the lower thoracolumbar spinal cord (Fig. 4*G,I,K,M,O,Q*) (counts for GFP$^+$ infection are from 15 or 16 sections per spinal cord region). We found that thoracolumbar CC neurons targeted multiple lobules (II-V, VIII) (GFP$^+$ (green) and GFP$^+$TOM$^+$ (yellow), Fig. 4*H–H′′′,J-J′′′,L-L′′′,N,P,R*, coronal and sagittal sections, $n = 3$ each, 1 F:2 M for coronal sections, 2 F:1 M for sagittal sections). Although there were discrete areas that did not contain GFP$^+$ cells (arrowheads, Fig. 4*H–H′′′,J-J′′′,L-L′′′*), GFP$^+$ cells were found over multiple lobules, indicating that CC axonal projections from the thoracolumbar spinal cord terminate throughout the cerebellar cortex, consistent with a discontinuous somatotopic map. Examples of GFP$^+$ (green, arrowheads) and GFP$^+$TOM$^+$ (white, arrows) MF terminals in lobules III and VIII in both coronal and sagittal sections are shown (Fig. 4*S,T*). In addition to terminating across several lobules, we found multiple examples of single axons terminating at regular intervals (50-80 µm) within a GC layer, which has been reported anecdotally in the literature (Reeber et al., 2011; Houck and Person, 2015; Gilmer and Person, 2017; Luo et al., 2018), indicating that a single CC neuron synapses on several GCs (Fig. 4*C–F*). Interestingly, an individual GC is ~40-50 µm from dendrite to dendrite (Gray, 1961; Eccles et al., 1967; Jakab and Hamori, 1988; Huang et al., 2013). Therefore, individual MF axons from a single CC neuron likely do not synapse on the same GC, suggesting that GCs are multimodal encoders at the single-cell level (Marr, 1969; Albus, 1971). Overall, we find that CC neurons arborize extensively within the cerebellar cortex, reaching targets over multiple lobules, rather than in clustered locations.

Atoh1-lineage neurons make the spino-LRt and spino-olivary tracts

Given that *Atoh1*-lineage neurons made few direct spinocerebellar neurons, we sought to identify where in the hindbrain *Atoh1*-lineage axons project. We pursued an intersectional genetic strategy to restrict somatic labeling to caudal *Atoh1*-lineage neurons (*Atoh1^{Cre}; Cdx2::FLPo; Ai65*) (Fig. 5*A*). Most prominently, we found dense projections of caudal *Atoh1*-lineage neurons in the LRt and IO (Fig. 5*E-H′*). To identify whether caudal *Atoh1*-lineage axons synapse on localized areas of the LRt and IO, we injected FG into the cerebellar AZ (Fig. 5*A,B*), which retrogradely labeled LRt MF and IO CF cell bodies. We found that caudal *Atoh1*-lineage axons target almost the entirety of the LRt and restricted areas of the IO (dorsal fold of the dorsal accessory olive [dfDAO], dorsal accessory olive [DAO], subnucleus a of the caudal medial accessory olive [cMAO^a], subnucleus b of cMAO [cMAO^b]) (Fig. 5*E′–H′*). Consistent with our findings, anterograde tracing in rats reports that the spino-olivary tract terminates in the DAO, cMAO^a, and cMAO^b (Swenson and Castro, 1983b; Matsushita et al., 1992; Oldenbeuving et al., 1999). Caudal *Atoh1*-lineage axons colocalize with the presynaptic marker VG2 and are in close apposition to FG labeled neurons in the LRt and IO indicative of synaptic connections (arrows, Fig. 5*I,J*; Movies 3 and 4). Axon terminations in the LRt and IO were verified in four caudal *Atoh1*-lineage mice. Moreover, TOM$^+$ terminals in a cleared brain of *Atoh1^{Cre}; Cdx2::FLPo; Ai65* mice are quite dense in the LRt and IO (Movie 5). Together, we find that spinal cord *Atoh1*-lineage neurons make the spino-LRt and spino-olivary tracts.

In the caudal *Atoh1*-lineage mice, a few places of expression are worth noting. First, the sensory neurons misexpress tdTomato, and their axons can be seen terminating in the dorsal horn of the cleared spinal cord (Movie 6). *Atoh1* is not known to be expressed in sensory neurons and we do not see sensory neurons labeled in *Atoh1$^{P2A\text{-}FLPo}$* mice, whose expression overlaps

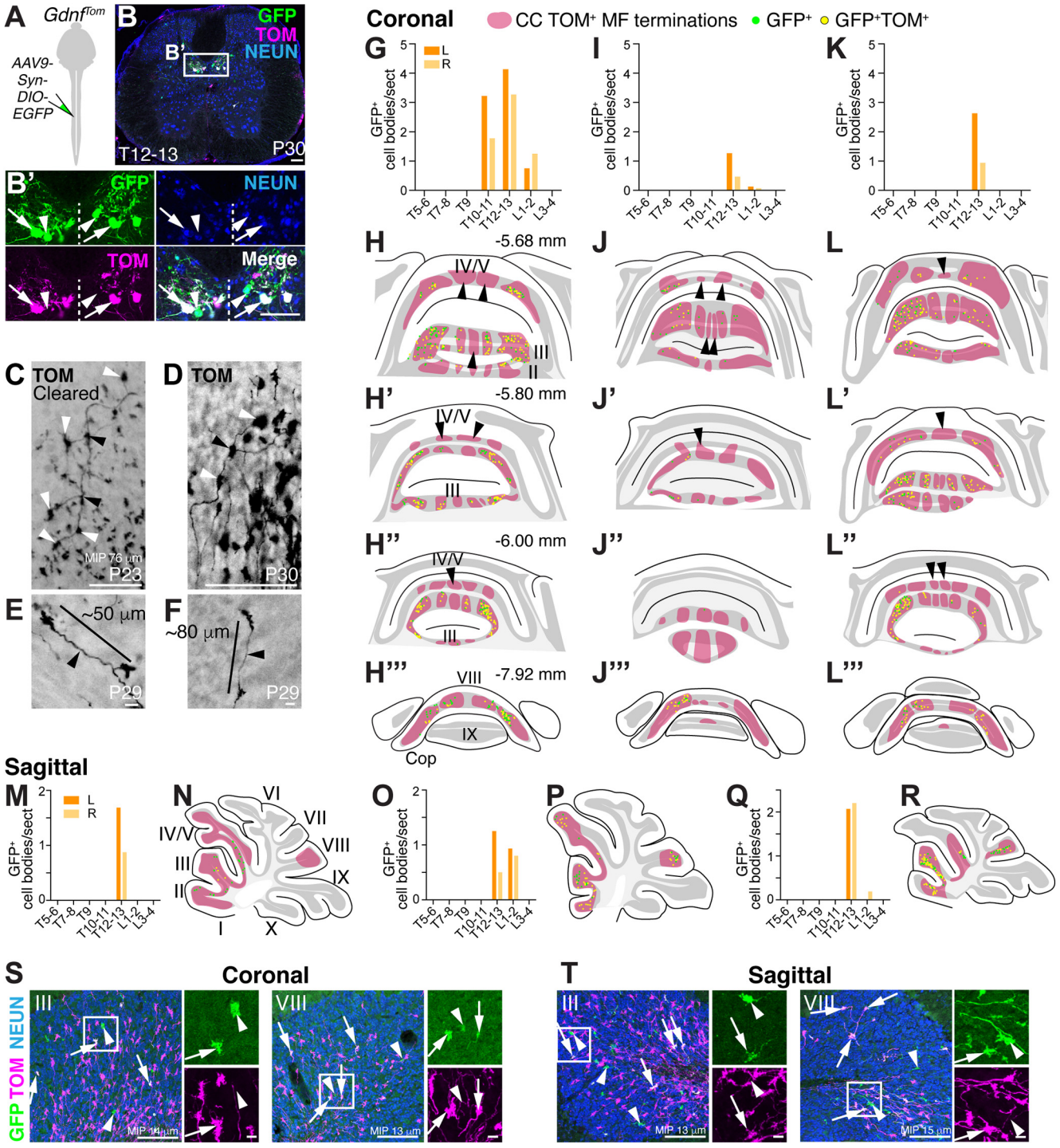

Figure 4. Thoracolumbar CC MFs send diverse projections to multiple lobules. ***A-B'***, Spinal cord injections of AAV9-Syn-DIO-EGFP at lower thoracic levels into *Gdnf*^{Tom} mice labels CC neurons on both sides of the spinal cord (***B'***). Arrows indicate GFP$^+$TOM$^+$. Arrowheads indicate GFP$^+$ only. ***C-F***, Examples of individual MF axons and terminals from 3 mice: a cleared female mouse sample (***C***, 76 µm MIP), 1 female mouse (***D***, 40 µm cryosection), and 1 male mouse (***E,F***, 40 µm cryosection). Axons appear to have branching points (black arrowheads) and regularly spaced MF terminals (white arrowheads) (***C,D***). MF terminals from an individual axon are spaced 50-80 µm apart (***E,F***). ***G-R***, MF terminations from thoracolumbar injections of *Gdnf*^{Tom} mice were analyzed in coronal and sagittal sections. Distribution of GFP$^+$ cells in the spinal cord on left (orange) and right (light orange) sides (***G,I,K,M,O,Q***). Schematics of coronal cerebellar sections from the spinal cord injections (***G,I,K***) indicating the location of CC MF terminations (***H-H'''*** / ***J-J'''*** / ***L-L'''***, TOM$^+$, red areas, respectively). Schematics of sagittal cerebellar sections from the spinal cord injections (***M,O,Q***) indicating the location of CC MF terminations (***N,P,R***, red areas, respectively). The subset of CC MF terminations that are from the lower thoracic-lumbar region (green represents GFP$^+$; yellow represents GFP$^+$TOM$^+$) are spread over multiple lobules (II-V, VIII). Certain CC MF termination regions do not have thoracolumbar CC neuronal projections (red areas, arrowheads with an absence of any GFP$^+$ terminations). ***S***, ***T***, Examples of CC MF terminations (arrows indicate GFP$^+$TOM$^+$; arrowheads indicate GFP$^+$-only) in lobules III and VIII from 13 to 15 µm MIP. Scale bars: ***B***, ***B'***, ***C***, ***D***, ***S***, ***T***, 100 µm; ***E***, ***F***, 10 µm.

quite well with the *Atoh1*^{Cre} knockin mouse for spinal cord interneurons (data not shown; Ogujiofor et al., 2021). Therefore, the sensory neuron labeling is because of misexpression of the CRE recombinase in sensory neurons. As a result, axons from sensory neurons going to the gracile, cuneate, and external cuneate nuclei can be seen in the cleared brain of *Atoh1*^{Cre}; *Cdx2::FLPo; Ai65* mice (Movie 5). Second, we find sparse ectopic labeling of *Atoh1*-lineage spinal vestibular (SpVe) soma in the hindbrain

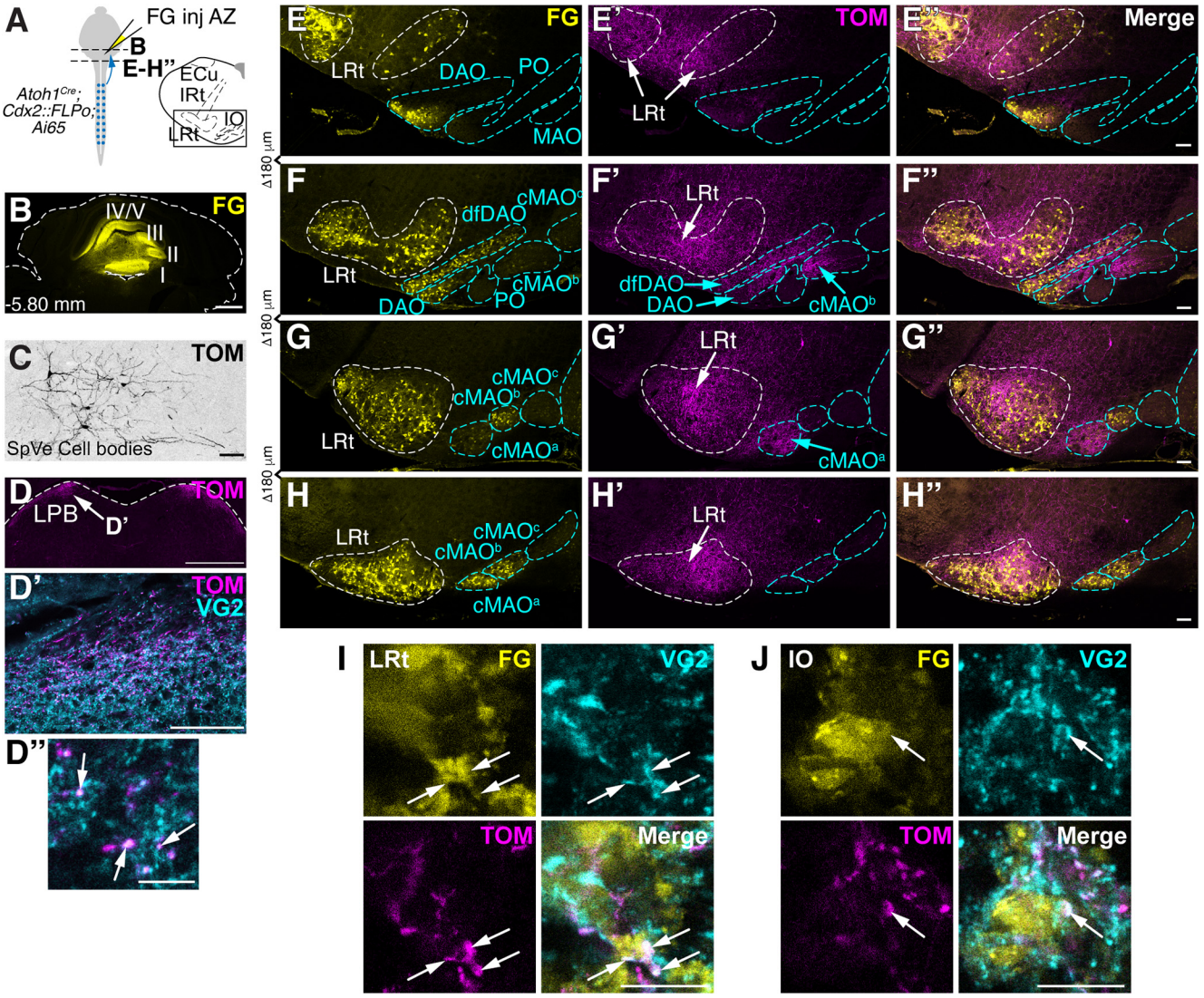

Figure 5. Spinal cord *Atoh1*-lineage neurons make spino-LRt and spino-olivary pathways. ***A***, Schematic of FG injections into the AZ of mice to identify LRt and IO neurons in the medulla. Axons of caudal *Atoh1*-lineage neurons are genetically labeled (*Atoh1*^{Cre}*; Cdx2::FLPo; Ai65* mice). ***B***, FG injected into lobules I-V. ***C***, Sparse cell bodies in the SpVe are detected in *Atoh1*^{Cre}*; Cdx2::FLPo; Ai65* mice. ***D-D′′***, TOM^{+} terminals seen in the lateral parabrachial (LPB) nucleus (***D***) are VG2^{+} (***D′′***, arrows). ***E-H′′***, A high density of caudal *Atoh1*-lineage axons from the spinal cord is found in the LRt as well as areas of the IO (dfDAO, DAO, cMAO^{a}, cMAO^{b}). ***I, J***, Caudal *Atoh1*-lineage axon terminals (TOM^{+}, magenta) expressing the presynaptic VG2 marker (cyan) are closely apposed to retrogradely labeled FG^{+} cells in the LRt (***I***) and IO (***J***) (arrows). Axonal terminations in the LRt and IO were verified in $n = 4$ mice. ***E-H′′***, Representative sections. ECu, External cuneate nucleus; cMAO^{a}, subnucleus a of caudal medial accessory olive; cMAO^{b}, subnucleus b of caudal medial accessory olive; cMAO^{c}, subnucleus c of caudal medial accessory olive; MAO, medial accessory olive; DAO, dorsal accessory olive; dfDAO, dorsal fold of the DAO; PO, principal olive; IRt, intermediate reticular nucleus; LRt, lateral reticular nucleus. Scale bars: ***B***, ***D***, 1 mm; ***C***, ***D′***, ***E-H′′***, 100 μm; ***D′′***, ***I***, ***J***, 10 μm.

(Fig. 5*C*) (Rose et al., 2009). SpVe neurons send descending projections to the spinal cord (Liang et al., 2015); therefore, we do not expect that this sparse ectopic labeling interferes with our analysis of ascending projections from caudal spinal cord *Atoh1*-lineage neurons. Last, we detect some TOM^{+} axons in the lateral parabrachial nucleus in *Atoh1*^{Cre}*; Cdx2::FLPo; Ai65* mice (TOM^{+}VG2^{+}, Fig. 5*D-D′*). Further studies are needed to determine exactly from where in the spinal cord these LPB projections originate and if they are truly *Atoh1*-lineage neurons or ectopic expression.

Spino-LRt and spino-olivary axonal projections originate from cervical *Atoh1*-lineage neurons

We pursued both retrograde and anterograde tracing strategies to determine which caudal *Atoh1*-lineage neurons contribute to the spino-LRt and spino-olivary tracts. In four different FG injections targeting the LRt and IO in *Atoh1*^{Tom} mice, we found that the retrogradely labeled *Atoh1*-lineage cells resided mainly in the cervical to upper thoracic areas (Fig. 6*A–G*, light purple, left side, and light blue, right side, FG^{+}TOM^{+} cells quantitated in Fig. 6*B,C,E,F*; $n = 4$, 3 F:1 M, 5 sections counted per spinal cord region, 7-9 weeks old). *Atoh1*-lineage neurons have previously been described as clustering into lateral and medial populations, which are thought to make up ipsilaterally and contralaterally projecting populations, respectively (Bermingham et al., 2001; Wilson et al., 2008; Yuengert et al., 2015). Retrogradely labeled neurons from the LRt and IO colocalized with both the lateral (Fig. 6*D′*,*G′*) and medial (Fig. 6*G′′*) *Atoh1*-lineage neurons. Because of the spread of the FG to both the LRt and IO, the precise ipsilateral or contralateral projections from either tract were not clear, but *Atoh1*-lineage neurons both ipsilateral (Fig. 6*G′*) and contralateral (Fig. 6*G′′*) to the injection site

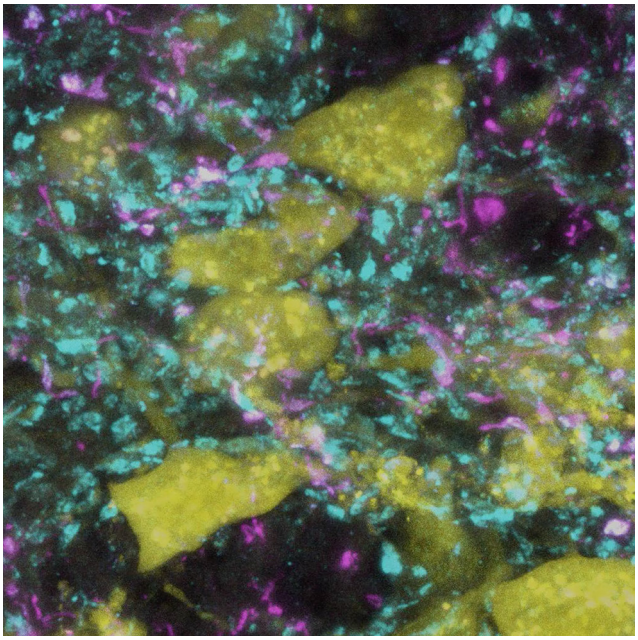

Movie 3. Three-dimensional projection of cells in the LRt of *Atoh1*^{Cre}*; Cdx2::FLPo; Ai65* mice. Cropped cell in Figure 5*I* is taken from this *z* stack of 0.5 µm optical slices with 0.25 µm step. Dense terminations are seen in the LRt. Yellow represents FG. Magenta represents *Atoh1*^{Cre}*; Cdx2::FLPo; Ai65* axons (TOM^{+}). Cyan represents VG2. [View online]

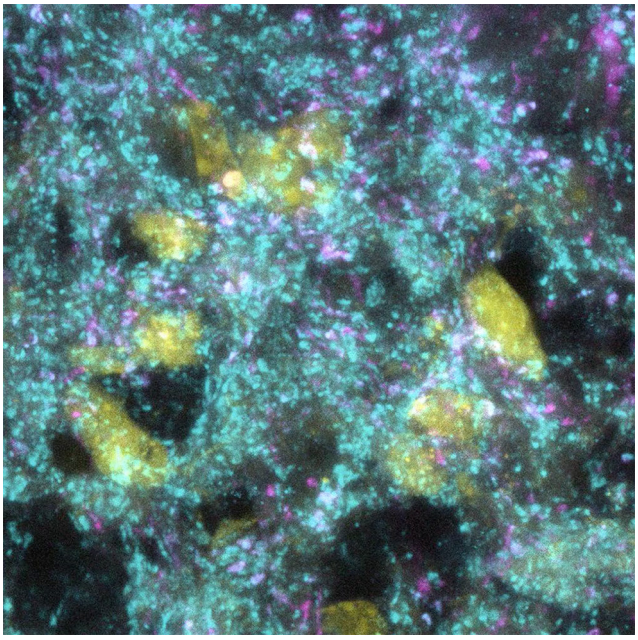

Movie 4. Three-dimensional projection of cells in the IO of *Atoh1*^{Cre}*; Cdx2::FLPo; Ai65* mice. Cropped cell in Figure 5*J* is taken from this *z* stack of 0.5 µm optical slices with 0.25 µm step. Dense terminations are seen in the IO. Yellow represents FG. Magenta represents *Atoh1*^{Cre}*; Cdx2::FLPo; Ai65* axons (TOM^{+}). Cyan represents VG2. [View online]

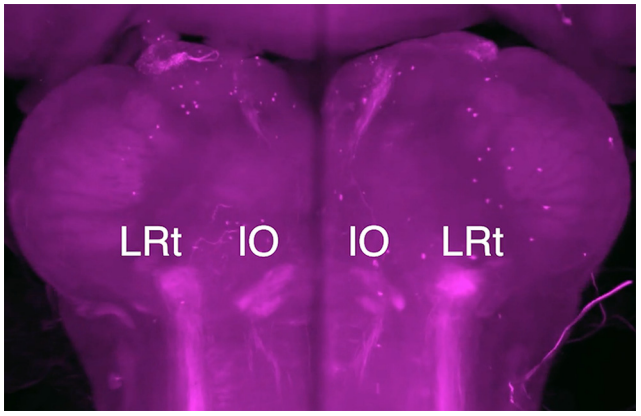

Movie 5. *Atoh1*^{Cre}*; Cdx2::FLPo; Ai65* cleared brain. The most prominent axonal projections in *Atoh1*^{Cre}*; Cdx2::FLPo; Ai65* mice are to the LRt and IO. Although MF projections are seen in cryosections, they are not obvious in the cleared spinal cord. There is diffuse tdTomato fluorescence in the thalamus and cortex. The misexpression of tdTomato in sensory neurons seen in the spinal cord is seen as projections to the cuneate (Cu), gracile (Gr), and external cuneate nucleus (ECu). [View online]

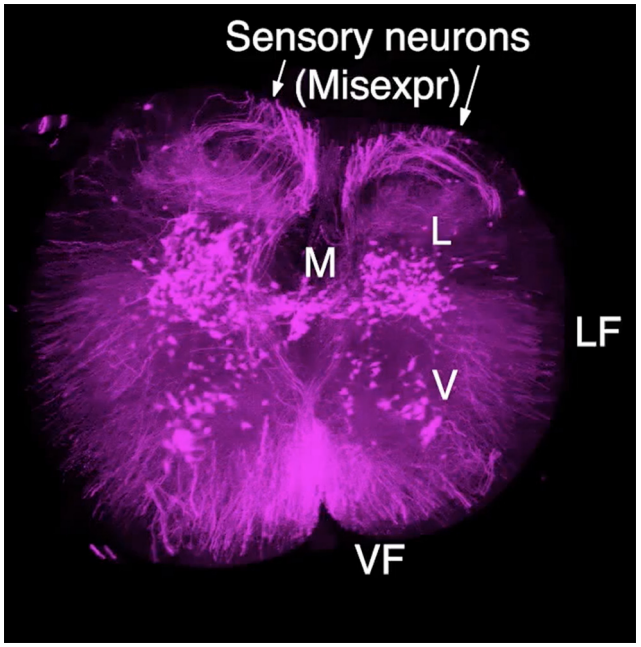

Movie 6. *Atoh1*^{Cre}*; Cdx2::FLPo; Ai65* cleared spinal cord. *Atoh1*-lineage neurons in the spinal cord cluster into medial (M), lateral (L), and ventral (V) populations whose axons travel in the LF and VF. tdTomato is misexpressed in sensory neurons. [View online]

were retrogradely labeled. Given the large number of neurons retrogradely labeled from the LRt and IO that are not *Atoh1*-lineage suggests that there are many other progenitor domains and cell types that contribute to these tracts (Alstermark and Ekerot, 2013; Azim et al., 2014; Pivetta et al., 2014; Jiang et al., 2015; Choi et al., 2020).

To identify the axonal projection targets of cervical *Atoh1*-lineage neurons, we pursued an intersectional strategy injecting Lenti$^{FugE\text{-}Cre}$ into the cervical area of *Atoh1*$^{P2A\text{-}FLPo}$ mice crossed to an intersectional tdTomato reporter (*Ai65*) (Fig. 6*H*). In 1 mouse, the infected neurons were restricted to the right spinal cord (Fig. 6*I*, *J*) and in another mouse, the infected cells were on both the left and right sides (Fig. 6*L*,*M*) ($n = 2$ male mice, 8-15 sections counted per spinal cord region, P30). In the mouse with the injection restricted to the right side, prominent axons were seen in the right LRt and the TOM^{+} terminations express VG2 (Fig. 6*K*-*K*′), suggesting that minimally, the spino-LRt *Atoh1*-lineage neurons are ipsilaterally projecting. In the other mouse that had TOM^{+} cells on both sides of the spinal cord, likely because of the virus being taken up by contralaterally projecting *Atoh1*-lineage neurons, we found axonal terminations in the right LRt and right cMAOb that were VG2^{+} and closely apposed to the postsynaptic density protein (PSD-95^{+}),

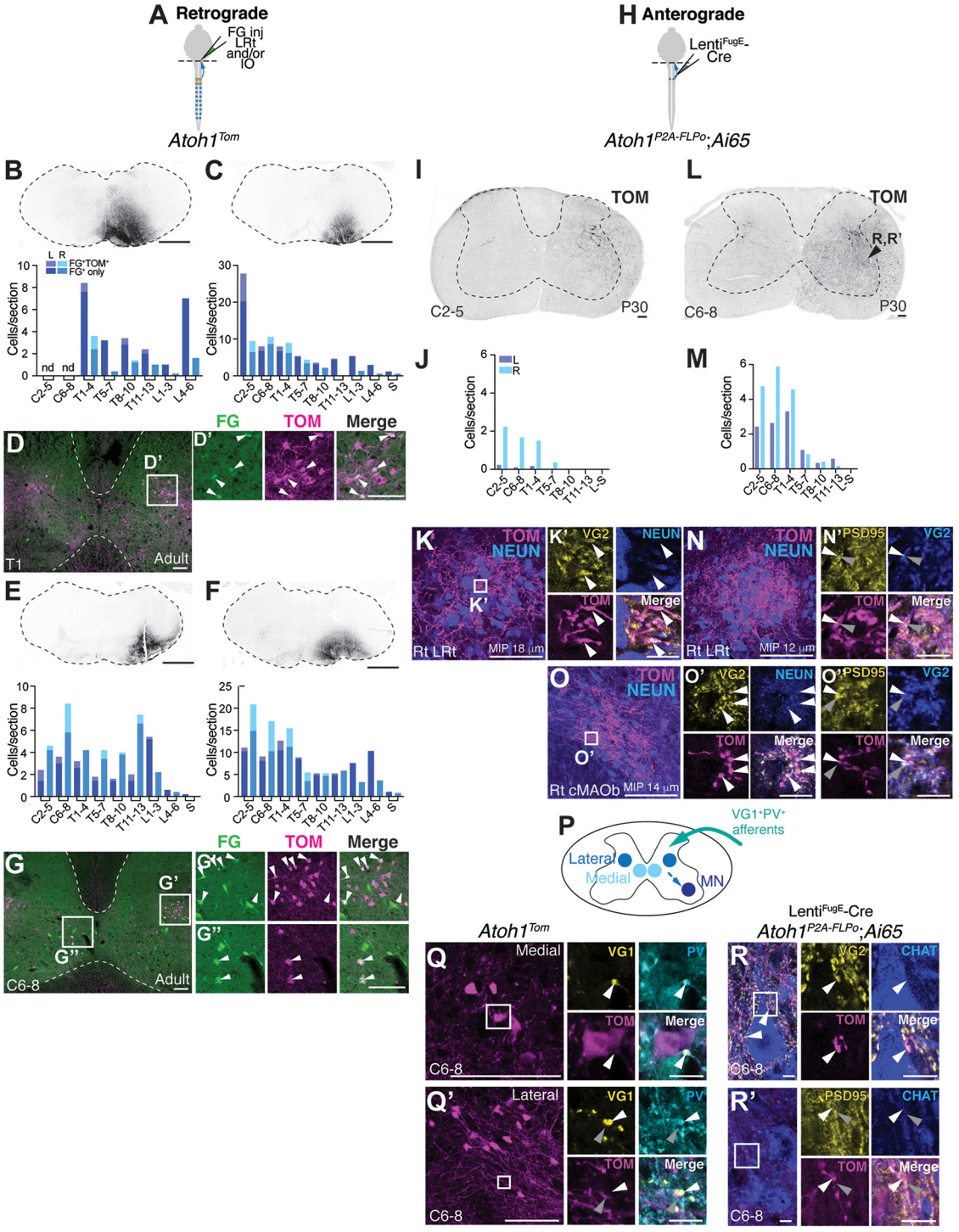

Figure 6. Cervical spinal cord *Atoh1*-lineage neurons project to the LRt and IO. ***A***, Schematic of FG injections into the right LRt and IO of *Atoh1*^{Tom} mice. ***B-G***, Retrogradely labeled *Atoh1*-lineage neurons reside mainly in the cervical to upper thoracic levels. Four injections targeting the LRt and IO in the medulla are shown (***B***,***C***,***E***,***F***, top panels). The spinal cords of these four injections have dual-labeled cells (FG^{+}TOM^{+}) mainly in the cervical to upper thoracic regions (light purple represents left side; light blue represents right side) with many other FG^{+} only cells elsewhere in the spinal cord (dark purple represents left side; dark blue represents right side). Representative spinal cord sections of the injection in ***C*** are shown in ***D-D′***, and the injection in ***F*** is shown in ***G-G′′***. *Atoh1*-lineage neurons in both the medial (***G′′***) and lateral (***D′***,***G′***) clusters are retrogradely labeled with FG (arrowheads). ***H***, Schematic of dual recombinase anterograde tracing. Lenti^{FugE}-Cre was injected into the right cervical spinal cord of *Atoh1*$^{P2A\text{-}FLPo}$; *Ai65* mice. ***I-O′′***, Anterograde tracing of *Atoh1*-lineage neurons finds axons in the LRt and IO. Injection of the right spinal cord (***I***) where mostly neurons on the right side are labeled (***J***) has axonal projections to the right LRt, which express the presynaptic marker VG2 (***K***,***K′***, arrowheads). Injection of the right spinal cord (***L***) where *Atoh1*-lineage neurons on both the left and right are labeled (***M***) has axonal projections to both the right LRt and IO, specifically the cMAOb (***N***,***O***). The *Atoh1*-lineage axonal terminals (TOM^{+}) express the presynaptic marker VG2 (white arrowheads) and are closely apposed to postsynaptic PSD95^{+} puncta (gray arrowheads) (***N′***,***O′***,***O′′***). Immunostaining for ***N′*** and ***O′′*** is performed on adjacent sections to ***N*** and ***O***. Images are taken from a similar axon dense region of the adjacent section. ***P***, Schematic of inputs and local outputs of cervical *Atoh1*-lineage neurons. ***Q***, ***Q′***, Synaptic terminals of proprioceptive afferents (VG1^{+}PV^{+}, white arrowheads) are closely apposed to TOM^{+} signal near medial and lateral *Atoh1*-lineage neurons. ***R***, ***R′***, Axons of cervical *Atoh1*-lineage neurons synapse on MNs (VG2^{+}TOM^{+} puncta closely apposed to PSD95^{+} puncta on CHAT^{+} MNs, white and gray arrowheads). CHAT^{+} neurons in ***R*** and ***R′*** were imaged from the area of the spinal cord indicated in ***L***. nd, Not determined. Scale bars: ***B***, ***C***, ***D***, ***D′***, ***E***, ***F***, ***G-G′′***, ***I***, ***K***, ***L***, ***O***, ***Q***, ***Q′***, 100 µm; ***K′***, ***N′***, ***O′***, ***O′′***, ***Q***, ***Q′***, high magnification, ***R***, ***R′***, high magnification, 10 µm.

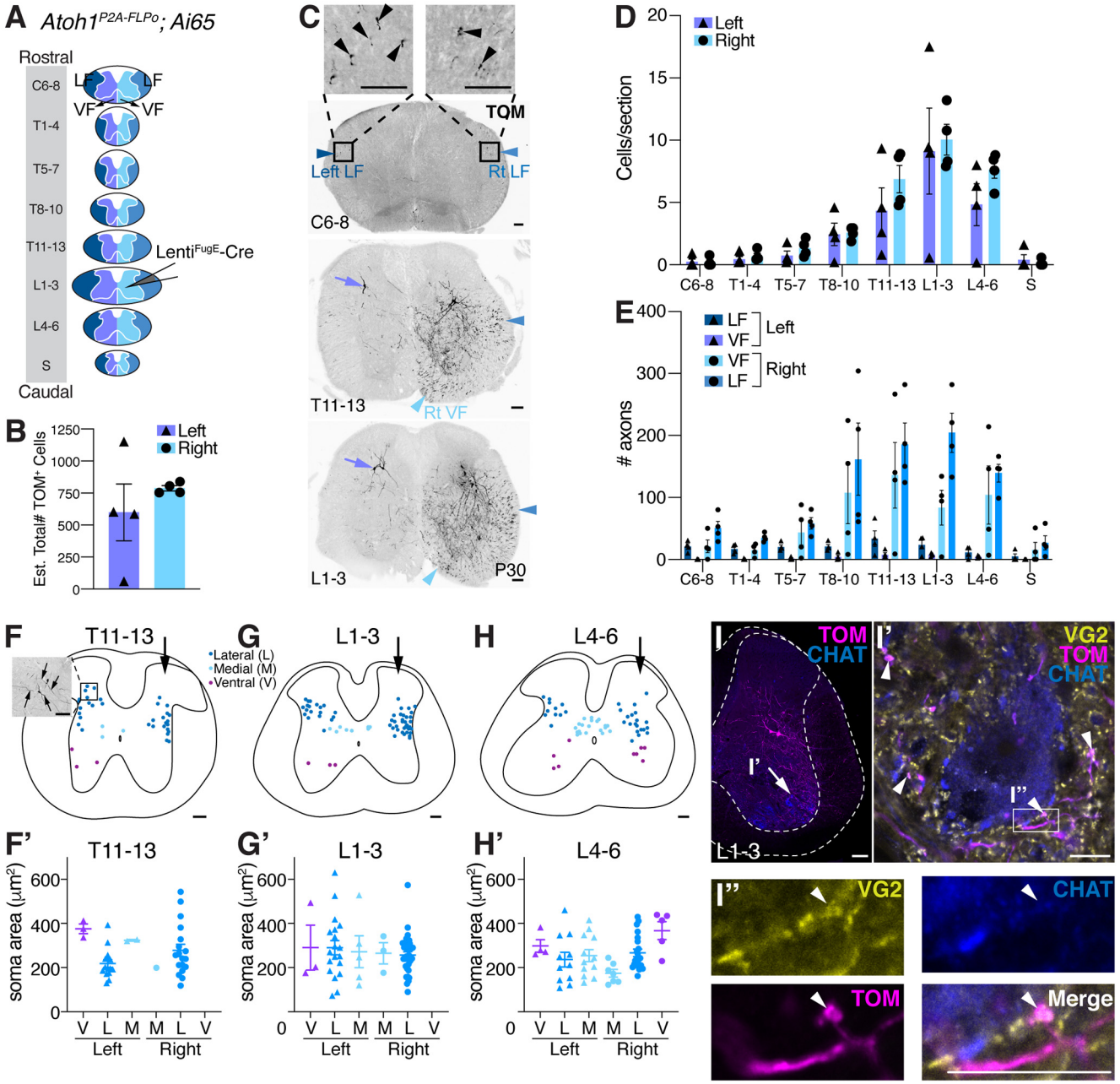

Figure 7. Thoracolumbar *Atoh1*-lineage neurons project locally within the spinal cord. ***A***, Diagram of rostral to caudal sections of the spinal cord (LF, dark blue represents left; blue represents right), gray matter, and VF (purple represents left; light blue represents right). Lenti^{FugE}-Cre was injected into *Atoh1*$^{P2A\text{-}FLPo}$*;Ai65* mice, such that *Atoh1*-lineage neurons in the right thoracolumbar spinal cord were labeled. ***B***, Quantitation of the total estimated number of infected cells (TOM$^+$) on the left and right sides. The virus appears to be taken up by axons of passage that project from the contralateral side (see ***C***). ***C***, Representative sections of the spinal cord from a Lenti^{FugE}-Cre-injected *Atoh1*$^{P2A\text{-}FLPo}$*;Ai65* mouse. Cell bodies on the right side of the spinal cord and axons in the right (Rt) LF (blue arrowhead) are labeled. Axons in the right ventral funiculus (Rt VF, light blue arrowhead) appear to be axons from cell bodies that are located on the contralateral side of the spinal cord (purple arrows). Some axons in the left LF (dark blue arrowhead) are also seen. ***D***, L1-3 is the site of peak infection (number of TOM$^+$ cell bodies labeled per section), and the number of cell bodies labeled tapers off both rostrally and caudally further away from the injection site. ***E***, Very few axons on the right side (blue represents LF; light blue represents VF) are detected in rostral sections (C6-8) compared with the site of injection L1-3. ***F-H'***, Distribution of infected cells in T11-13, L1-3, and L4-6 regions of the spinal cord (***F***,***G***,***H***, arrows indicate injection on right side). Quantitation of the soma area size of infected medial (M), lateral (L), and ventral (V) *Atoh1*-lineage neurons on the left and right sides of the spinal cord (***F'***,***G'***,***H'***). ***F***, Inset, Two cell bodies labeled on the left side contralateral to the injection that have projections extending dorsolaterally and medioventrally (arrows). ***I-I''***, Some of the sparsely labeled thoracolumbar *Atoh1*-lineage neurons have presynaptic terminals near (TOM$^+$VG2$^+$, arrowheads) or closely apposed (***I''***, TOM$^+$VG2$^+$, arrowhead) to MNs (CHAT$^+$) (detected in $n = 4$ samples, representative image shown). For details of quantitation for ***B***, ***D***, ***E***, ***F'***, ***G'***, and ***H'***, see Materials and Methods and Results. Scale bars: ***C***, ***I***, 100 μm; ***I'***, ***I''***, 10 μm. Results in graphs are mean ± SEM.

suggesting that these are functional excitatory synapses (Fig. 6*N–O''*, TOM$^+$VG2$^+$, white arrowheads; PSD95$^+$, gray arrowheads).

We next examined the local inputs and outputs of cervical *Atoh1*-lineage neurons. We had previously shown that thoracolumbar *Atoh1*-lineage neurons receive proprioceptive input (Yuengert et al., 2015). Here, we found that both medial and lateral *Atoh1*-lineage neurons in the cervical area (TOM$^+$) have processes closely apposed to VG1$^+$ and parvalbumin (PV$^+$) synapses indicative of proprioceptive afferents (Fig. 6*Q–Q'*). Similar to our previous results for the thoracolumbar *Atoh1*-lineage

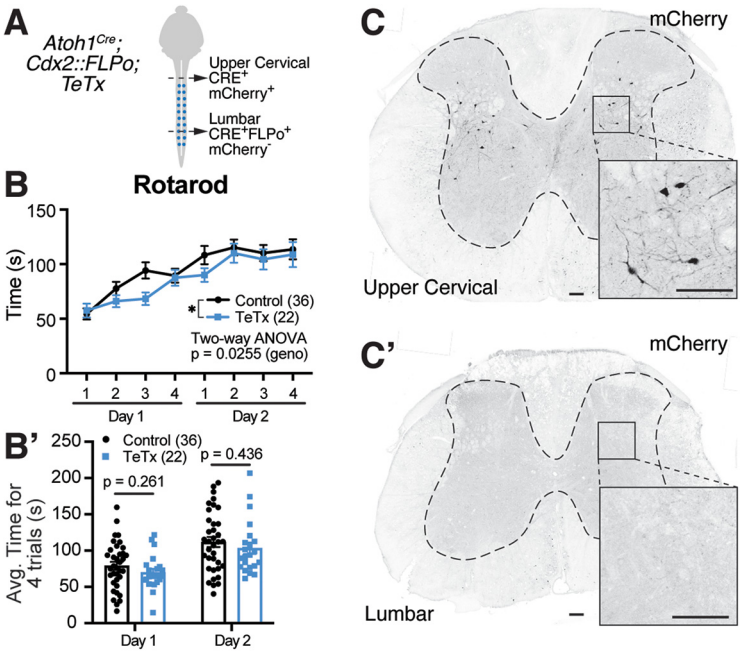

Figure 8. Sparse silencing of caudal *Atoh1*-lineage neurons leads to an inconclusive phenotype. ***A***, Schematic of dual recombinase strategy to silence caudal *Atoh1*-lineage neurons. ***B***, Mice heterozygous for the TeTx allele in caudal *Atoh1*-lineage neurons had an inconclusive phenotype in the rotarod assay (two-way ANOVA, $F_{(1,448)} = 5.025$, $p = 0.0255$ for genotype; Bonferroni *post hoc* test found no significant multiple pairwise comparisons). Control: $n = 36$ (20 F:16 M), TeTx: $n = 22$ (10 F:12 M). ***B'***, Comparison of the average times for Trials 1-4 on days 1 and 2 between control and TeTx mice was not significant (unpaired, parametric, two-tailed Student's *t* test). ***C***, ***C'***, Upper cervical areas of the spinal cord in *Atoh1*^{Cre}*;Cdx2::FLPo; TeTx* mice only have *Atoh1*^{Cre} expressed and are thus mCherry$^+$ (***C***). Lumbar areas of the spinal cord that have both *Atoh1*^{Cre} and *Cdx2::FLPo* expressed have lost the mCherry signal (***C'***). ***C***, ***C'***, mCherry signal was amplified using a dsRed antibody. Scale bars: ***C***, ***C'***, 100 μm.

neurons (Yuengert et al., 2015), we were able to visualize axo-somatic synapses for the medial population (Fig. 6*Q*, VG1$^+$PV$^+$, white arrowhead), but we were unable to identify axo-somatic synapses on the lateral population. We could only find VG1$^+$PV$^+$ afferents passing near TOM$^+$ processes in the vicinity of the lateral soma (Fig. 6*Q'*, VG1$^+$PV$^+$, white arrowhead; TOM$^+$, gray arrowhead). Last, we found that the axons of sparsely labeled cervical *Atoh1*-lineage neurons made synapses on motor neurons (MNs) (Fig. 6*R–R'*). Together, we found that cervical *Atoh1*-lineage neurons can receive proprioceptive input and do indeed project to the LRt and IO as well as locally to MNs in the cervical spinal cord.

Thoracolumbar *Atoh1*-lineage neurons project locally

We next examined whether sparsely labeled thoracolumbar *Atoh1*-lineage neurons send axonal projections to the medulla or cerebellum. Using the same intersectional injection strategy, except with the Lenti$^{FugE\text{-}Cre}$ targeted to the right thoracolumbar spinal cord (light blue), we again found several cell bodies on the contralateral side labeled (Fig. 7*B*; 786 ± 20 cells, right side vs 598 ± 223 cells, left side; $n = 4$, 3 F:1 M, total number of cells infected was estimated from counts of 20% of each spinal cord region), which is likely because of the virus being taken up by axons of passage projecting contralaterally (Fig. 7*C*, axons labeled in the right ventral funiculus, light blue arrowhead). Most of the cell bodies labeled were in the thoracolumbar area (Fig. 7*D*) (cell bodies counted from 13-30 sections per spinal cord region). Strikingly, we found that axons in the right ventral funiculus (VF) and LF decreased both rostrally and caudally, suggesting that most of these axons are local projections (Fig. 7*E*) (axons counted from the right and left LF and VF from one section/spinal cord region) and that few thoracolumbar *Atoh1*-lineage neurons project to the LRt, IO, and cerebellar cortex.

Interestingly, the neurons labeled on the left side of the spinal cord, contralateral to the injected side, were located more dorsolaterally than expected for the medial *Atoh1*-lineage population that is known to project contralaterally (Fig. 7*C*, purple arrows) (Bermingham et al., 2001; Wilson et al., 2008; Yuengert et al., 2015). This observation prompted us to characterize the distribution and cell soma size of infected *Atoh1*-lineage neurons (Fig. 7*F–H'*). In the spinal cord areas of peak infection (T11-13, L1-3, and L4-6), we found that medial, lateral, and the ill-described ventral *Atoh1*-lineage populations on both sides of the spinal cord were labeled (Fig. 7*F–H*, $n = 4$, 3-6 sections/*n*). Quantitation of the soma area found no size differences between the lateral, medial, and ventral population on either side (one-way ANOVA of clusters that had $n > 5$ cells). We believe that the cells infected on the left side are labeled through their contralaterally projecting axons that take up the virus on the right side. This suggests that at least a subset of lateral *Atoh1*-lineage cells can also project contralaterally. Indeed, imaging of some of the neurons on the left side shows processes projecting both ventromedially and dorsolaterally (Fig. 7*F*, inset, arrows), suggesting that these neurons could project both ipsilaterally and contralaterally. While it is possible that cells labeled on the left side are because of diffusion of the virus across the midline, we would have expected the lateral *Atoh1*-lineage neurons in this scenario to project ipsilaterally; therefore, there should be almost equal numbers of axons in the left and right LF given that the number of soma on each side is similar. However, the number of axons in the left LF are low compared with the right LF (Fig. 7*E*). Therefore, we surmise that the neurons infected on the left side are contralaterally projecting lateral *Atoh1*-lineage cells, a subset of which could also project ipsilaterally.

Because of the dense ventral projections in our sparsely labeled *Atoh1*-lineage neurons (Fig. 7*C*, T11-13 and L1-3), we asked whether thoracolumbar *Atoh1*-lineage neurons also synapse on MNs. Similar to the cervical *Atoh1*-lineage neurons, we found in all four injections a high density of TOM$^+$VG2$^+$ puncta (Fig. 7*I-I'*, arrowheads) near and some very closely apposed to CHAT$^+$ MNs (Fig. 7*I''*, arrowhead). Some of these TOM$^+$VG2$^+$ puncta might be axo-dendritic synapses (Fig. 7*I'*, arrowheads), while only a few axo-somatic contacts are detected (Fig. 7*I''*). Thus, we find that thoracolumbar *Atoh1*-lineage neurons primarily project locally, where they synapse onto MNs, with few neurons projecting to higher brain regions.

Sparse expression of a silencing allele in caudal *Atoh1*-lineage neurons leads to an inconclusive motor phenotype

To understand how caudal *Atoh1*-lineage neurons affect motor behavior, we expressed a GFP-TeTx light chain fusion protein in these neurons to inhibit vesicle neurotransmission (Fig. 8*A*; *Atoh1*^{Cre}*;Cdx2::FLPo;R26*$^{LSL\text{-}FSF\text{-}TeTx}$) (Kim et al., 2009) and assessed their behavior in an accelerating rotarod assay. We

analyzed mice heterozygous for the TeTx allele because the *Atoh1* gene is close to the *ROSA* locus on chromosome 6; thus, homologous recombination occurs too infrequently to get homozygosity at the *ROSA* locus along with the $Atoh1^{Cre}$ allele. The way that the $R26^{LSL\text{-}FSF\text{-}TeTx}$ mouse was designed, CRE recombinase expression alone allows for mCherry expression while CRE and FLPo recombinase allows for expression of the GFP-TeTx fusion protein, but not mCherry (Kim et al., 2009). We confirmed in the behavioral cohort that all 22 test mice ($Atoh1^{Cre}$;*Cdx2::FLPo*;$R26^{LSL\text{-}FSF\text{-}TeTx}$) had nondysregulated mCherry expression in the upper cervical spinal cord and that the mCherry expression was absent in the lumbar spinal cord (Fig. 8*C*–*C*′). However, we were unable to detect GFP-TeTx at the mRNA or protein levels, although we believe it is sparsely expressed (for details, see Materials and Methods). Correspondingly, we found the phenotype on rotarod to be inconclusive (Fig. 8*B*, two-way ANOVA, $p = 0.0255$; for a main effect because of genotype, a Bonferroni *post hoc* test found no significant multiple pairwise comparisons). Further analysis of the data averaging the four daily trials for days 1 and 2 found no significant effect (Fig. 8*B*′, unpaired, parametric, two-tailed Student's *t* test). MNs involved in fine motor control are labeled in the $Atoh1^{Cre}$ mice so GFP-TeTx may be sparsely expressed in these MNs as well (Ogujiofor et al., 2021).

Discussion

In this study, we define the anatomy of proprioceptive spinal pathways and find surprising features of these ascending projections (summarized in Fig. 9). We find that CC neurons avoid significant collateralization within the spinal cord, medulla, and CN, although they do collateralize extensively within the cerebellar cortex with some axons crossing the midline. We also discover that cervical *Atoh1*-lineage neurons make up the indirect spino-LRt and spino-olivary pathways while thoracolumbar *Atoh1*-lineage neurons project mostly locally within the spinal cord. In contrast to CC neurons, cervical and thoracolumbar *Atoh1*-lineage neurons make direct connections to MNs. Together, we find that the proprioceptive circuits within the spinal cord consist of long-range direct (CC) as well as indirect and locally projecting (cervical and thoracolumbar *Atoh1*-lineage) neurons that likely mediate different aspects of proprioception.

Diversification of proprioceptive information through CC neurons

We find many unique anatomic features of CC neurons that lend insight into how proprioceptive information through CC neurons is relayed. First, we find that a couple thousand CC neurons make up 43%-47% of the direct DSCT and VSCT pathways from the AZ relaying hindlimb proprioceptive information. Second, our work clarifies that CC neurons synapse primarily on GCs and do not collateralize significantly within the spinal cord, medulla, or CN, which has been a matter of debate in the literature (Ekerot and Oscarsson, 1976; Szabo et al., 1990; Jiang et al., 2015; Luo et al., 2018). The fact that CC neurons do not collateralize to other parts of the brainstem or CN, as is seen for other MF terminal sources (Sillitoe et al., 2012; Beitzel et al., 2017) suggests that they are not involved in sending proprioceptive information to other ascending or descending proprioceptive-motor pathways, except at the GC level. Last, we do find, though, that within the cerebellar cortex, CC neurons extensively diversify their MF terminals between lobules, within a lobule, and even crossing the cerebellum to the contralateral side. Our estimate of ~72 MF terminals for 1 CC soma at a population level is similar to the reported 99 terminals/neuron for CC neurons from single-axon reconstructions (Luo et al., 2018). Part of the reason for this expansion of proprioceptive information could be for parallel processing across many domains of the cerebellar cortex.

Atoh1-lineage spino-LRt and spino-olivary neurons

We initially hypothesized that *Atoh1*-lineage neurons made lamina V-SCT or dhSCT neurons based on their anatomic location and developmental studies that reported *Atoh1*-lineage axons go to the cerebellum (Matsushita and Hosoya, 1979; Bermingham et al., 2001; Sakai et al., 2012; Yuengert et al., 2015). Instead, we found that cervical *Atoh1*-lineage neurons make mainly the indirect spino-LRt and spino-olivary pathways. Thus, the cerebellar axonal projections seen during development either extend to the cerebellum and retract during development or die. However, it is possible that *Atoh1*-lineage neurons make a subset of direct spinocerebellar neurons that project to the posterior zone (lobules VIII/IXa), which was not assessed in our study. Cervical *Atoh1*-lineage neurons could contribute to any of three possible spino-LRt populations that function in posture (bilateral ventral reflex tract), reaching (propriospinal), or grasping (ipsilateral forelimb tract) (Alstermark and Ekerot, 2013; Jiang et al., 2015). We found that cervical *Atoh1*-lineage neurons appear to target the LRt ipsilaterally and as a population can synapse on MNs as well; therefore, it seems likely that *Atoh1*-lineage neurons are at least propriospinal spino-LRt neurons. For the spino-olivary pathway, we found cervical *Atoh1*-lineage neurons targeted areas of the IO (dfDAO, DAO, $cMAO^{a}$, $cMAO^{b}$) consistent with previously described tracing studies and that retrograde tracing from the IO colocalizes with *Atoh1*-lineage neurons in laminae V-VIII (Swenson and Castro, 1983a,b; Matsushita et al., 1992; Oldenbeuving et al., 1999; Flavell et al., 2014). Overall, though, there are numerous other spino-LRt and spino-olivary neurons in the spinal cord, suggesting that there are additional sources that are not from the *Atoh1*-lineage (Azim et al., 2014; Pivetta et al., 2014; Choi et al., 2020).

Local projections of *Atoh1*-lineage neurons

We find some interesting features of locally projecting *Atoh1*-lineage neurons and compare and contrast our findings with those of a previous study using an *Atoh1*-enhancer driving CRE recombinase electroporated into mouse embryos (Kaneyama and Shirasaki, 2018). First, we find that thoracolumbar *Atoh1*-lineage neurons project mostly locally, consistent with the findings by Kaneyama and Shirasaki (2018), who found that crossing dI1 axons are intersegmental with only a few traveling far from the soma. Second, we found that *Atoh1*-lineage neurons in both the cervical and thoracolumbar areas of the mature spinal cord make local circuit connections with MNs as previously described during embryogenesis and are thus a source of premotor neurons (Goetz et al., 2015). Kaneyama and Shirasaki (2018) found that dI1 commissural axons made synapses on axial MNs, while we found that *Atoh1*-lineage neurons as a population can target the lateral motor column as well. Last, similar to our findings, they also found that some dI1 commissural axons come from a fairly dorsolateral population, rather than a medial population, and that these neurons in the lateral population appear to project both contralaterally and ipsilaterally.

Comparison of motor behaviors mediated by proprioceptive spinal pathways

Loss of proprioceptive input in animal models leads to defects in limb coordination and lack of adaptation to uneven surfaces

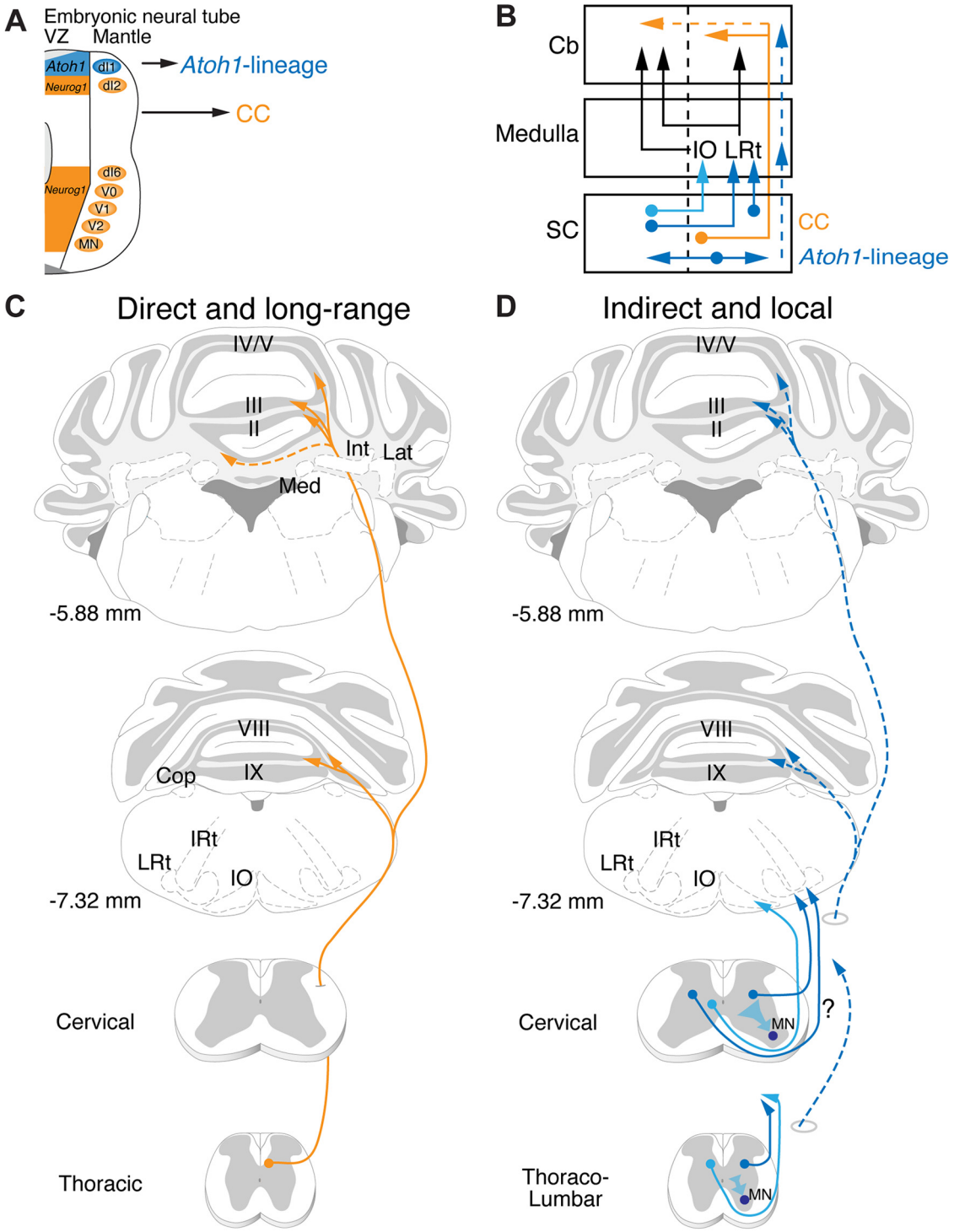

Figure 9. Long-range direct and local indirect proprioceptive pathways. ***A***, *Neurog1*-lineage neurons of the developing neural tube generate CC neurons that project directly from the spinal cord to the cerebellum while *Atoh1*-lineage neurons form mostly indirect spinocerebellar and local spinal projections. ***B***, Schematic of major anatomic findings. CC neurons (orange) project ipsilaterally mainly from the thoracic spinal cord directly to the cerebellum. Some CC axons cross the midline (dotted orange). Cervical *Atoh1*-lineage neurons project mainly to the LRt and IO in the medulla (dark and light blue). The LRt neurons then project either ipsilaterally or contralaterally to terminate in the cerebellar cortex as MFs. The neurons in the IO then project contralaterally as well to synapse as climbing fiber (CF) axons onto Purkinje cells (PCs) in the cerebellar cortex. Thoracolumbar *Atoh1*-lineage neurons project mostly within the spinal cord (dark blue, horizontal arrows), although a few project to more rostral regions within the medulla and cerebellum (dotted blue arrows). ***C***, ***D***, Illustrations of long-range direct and local indirect spinocerebellar pathways. CC neurons project rostrally in the ipsilateral funiculus where they branch extensively in the cerebellum, avoiding the medulla and CN (Med, Int, Lat) to terminate in vermis I-V, VIII, IXa, and Cop (C). Some CC axons cross the midline within the cerebellum. *Atoh1*-lineage neurons are heterogeneous with diverse projections. Cervical *Atoh1*-lineage neurons in the spinal cord project both ipsilaterally and contralaterally to target mainly the LRt and IO in the hindbrain (***D***). While we found that some of the *Atoh1*-lineage spino-LRt axons project ipsilaterally, whether some spino-LRt projections come from the contralateral side was not determined in this study (question mark along axons). The spino-IO tract is likely contralateral based on previous literature. *Atoh1*-lineage neurons in the thoracolumbar area project mostly locally within the spinal cord. A few of the axons from thoracolumbar *Atoh1*-lineage neurons may project to the medulla or cerebellar cortex (dotted blue). Presynaptic terminals from *Atoh1*-lineage neurons are found on MNs in both the cervical and thoracolumbar spinal cord. IRt, Intermediate reticular nucleus.

(Abelew et al., 2000; Windhorst, 2007; Akay et al., 2014). Differences in circuitry between CC (long-range) and caudal *Atoh1*-lineage neurons (indirect and local) suggest that different aspects of proprioceptive-motor behaviors could be mediated by separable microcircuits. We attempted to examine the function of caudal *Atoh1*-lineage neurons by expressing a silencing allele, tetanus toxin light chain. However, the phenotype was inconclusive on the accelerating rotarod, and we determined that the lack of phenotype was likely because of sparse expression of the GFP-TeTx allele.

Cervical *Atoh1*-lineage neurons also contribute to the spino-olivary tract. We are not aware of any studies that have manipulated the activity of spino-olivary neurons. However, mice that had glutamatergic signaling in IO neurons knocked out had dystonia-like features, such as twisting, stiff limbs, and tremor, and were unable to perform on the accelerating rotarod test (White and Sillitoe, 2017). Mice that had *Atoh1* knocked out caudal to the lower medulla did not exhibit any overt twisting, stiff limbs, or tremor, but they were similarly completely unable to perform the rotarod test (Yuengert et al., 2015). Therefore, the inability to update motor outcomes may be due in part to the contribution of *Atoh1*-lineage neurons to the spino-olivary system. Together, caudal *Atoh1*-lineage neurons are heterogeneous comprising parts of the spino-LRt and spino-olivary tracts as well as projecting locally within the spinal cord. Future experiments uncoupling the function of these different components using more robust ablation or acute silencing strategies will lend further insight into the function of discrete proprioceptive circuits.

Future directions

Our work and others suggest that the spinocerebellar and spino-LRt systems come from several developmental progenitor domains and that any given developmental progenitor domain (e.g., *Atoh1*) contributes to several neuronal types (minimally, spino-LRt and spino-olivary tracts, as well as local spinal neurons). Comparing and contrasting features of neurons with similar anatomic connectivity but generated from different progenitor domains may lend insights into the varied functions mediated by seemingly similar anatomic classes. Conversely, separating out different pathways, such as the spino-LRt and spino-olivary tracts that are generated from a single progenitor domain (*Atoh1*), will be important for determining the separate functions of these pathways.

We found that direct CC neurons do not send significant axon collaterals to the LRt or IO and that information to the LRt and IO is in part coming from *Atoh1*-lineage neurons. Therefore, the MF and CF input coming from the spinal cord into the cerebellar cortex comes from different information streams and are not simply collateral copies of the direct CC pathway. Future work focused on how the direct and indirect information streams from the spinal cord either converge or diverge within the cerebellar cortex, and the timing with which this information comes in from the two different information streams will be particularly interesting.

References

Abelew TA, Miller MD, Cope TC, Nichols TR (2000) Local loss of proprioception results in disruption of interjoint coordination during locomotion in the cat. J Neurophysiol 84:2709–2714.

Akay T, Tourtellotte WG, Arber S, Jessell TM (2014) Degradation of mouse locomotor pattern in the absence of proprioceptive sensory feedback. Proc Natl Acad Sci USA 111:16877–16882.

Albus JS (1971) Mathematical biosciences. Amsterdam: Elsevier.

Alstermark B, Ekerot CF (2013) The lateral reticular nucleus: a precerebellar centre providing the cerebellum with overview and integration of motor functions at systems level. A new hypothesis. J Physiol 591:5453–5458.

Apps R, Hawkes R (2009) Cerebellar cortical organization: a one-map hypothesis. Nat Rev Neurosci 10:670–681.

Arsenio Nunes ML, Sotelo C (1985) Development of the spinocerebellar system in the postnatal rat. J Comp Neurol 237:291–306.

Avraham O, Hadas Y, Vald L, Zisman S, Schejter A, Visel A, Klar A (2009) Transcriptional control of axonal guidance and sorting in dorsal interneurons by the Lim-HD proteins Lhx9 and Lhx1. Neural Dev 4:21.

Azim E, Jiang J, Alstermark B, Jessell TM (2014) Skilled reaching relies on a V2a propriospinal internal copy circuit. Nature 508:357–363.

Baek M, Menon V, Jessell TM, Hantman AW, Dasen JS (2019) Molecular logic of spinocerebellar tract neuron diversity and connectivity. Cell Rep 27:2620–2635.e2624.

Beitzel CS, Houck BD, Lewis SM, Person AL (2017) Rubrocerebellar feedback loop isolates the interposed nucleus as an independent processor of corollary discharge information in mice. J Neurosci 37:10085–10096.

Berkley KJ, Worden IG (1978) Projections to the inferior olive of the cat: I. Comparisons of input from the dorsal column nuclei, the lateral cervical nucleus, the spino-olivary pathways, the cerebral cortex and the cerebellum. J Comp Neurol 180:237–251.

Bermingham NA, Hassan BA, Wang VY, Fernandez M, Banfi S, Bellen HJ, Fritzsch B, Zoghbi HY (2001) Proprioceptor pathway development is dependent on Math1. Neuron 30:411–422.

Bosco G, Poppele RE (2001) Proprioception from a spinocerebellar perspective. Physiol Rev 81:539–568.

Bourane S, Grossmann KS, Britz O, Dalet A, Del Barrio MG, Stam FJ, Garcia-Campmany L, Koch S, Goulding M (2015) Identification of a spinal circuit for light touch and fine motor control. Cell 160:503–515.

Cebrian C, Asai N, D'Agati V, Costantini F (2014) The number of fetal nephron progenitor cells limits ureteric branching and adult nephron endowment. Cell Rep 7:127–137.

Choi S, Hachisuka J, Brett MA, Magee AR, Omori Y, Iqbal NU, Zhang D, DeLisle MM, Wolfson RL, Bai L, Santiago C, Gong S, Goulding M, Heintz N, Koerber HR, Ross SE, Ginty DD (2020) Parallel ascending spinal pathways for affective touch and pain. Nature 587:258–263.

Cummings JF, Petras JM (1977) The origin of spinocerebellar pathways: I. The nucleus cervicalis centralis of the cranial cervical spinal cord. J Comp Neurol 173:655–692.

Eccles JC, Ito M, Szentágothai J (1967) The cerebellum as a neuronal machine. New York: Springer.

Edgley SA, Gallimore CM (1988) The morphology and projections of dorsal horn spinocerebellar tract neurones in the cat. J Physiol 397:99–111.

Ekerot CJ, Oscarsson L (1976) The lateral reticular nucleus in the cat: V. Does collateral activation from the dorsal spinocerebellar tract occur? Exp Brain Res 25:327–337.

Flavell CR, Cerminara NL, Apps R, Lumb BM (2014) Spino-olivary projections in the rat are anatomically separate from postsynaptic dorsal column projections. J Comp Neurol 522:2179–2190.

Gebre SA, Reeber SL, Sillitoe RV (2012) Parasagittal compartmentation of cerebellar mossy fibers as revealed by the patterned expression of vesicular glutamate transporters VGLUT1 and VGLUT2. Brain Struct Funct 217:165–180.

Gilmer JI, Person AL (2017) Morphological constraints on cerebellar granule cell combinatorial diversity. J Neurosci 37:12153–12166.

Goetz C, Pivetta C, Arber S (2015) Distinct limb and trunk premotor circuits establish laterality in the spinal cord. Neuron 85:131–144.

Gordon J, Ghilardi MF, Ghez C (1995) Impairments of reaching movements in patients without proprioception: I. Spatial errors. J Neurophysiol 73:347–360.

Gowan K, Helms AW, Hunsaker TL, Collisson T, Ebert PJ, Odom R, Johnson JE (2001) Crossinhibitory activities of Ngn1 and Math1 allow specification of distinct dorsal interneurons. Neuron 31:219–232.

Gray EG (1961) The granule cells, mossy synapses and Purkinje spine synapses of the cerebellum: light and electron microscope observations. J Anat 95:345–356.

Hantman AW, Jessell TM (2010) Clarke's column neurons as the focus of a corticospinal corollary circuit. Nat Neurosci 13:1233–1239.

Houck BD, Person AL (2015) Cerebellar premotor output neurons collateralize to innervate the cerebellar cortex. J Comp Neurol 523:2254–2271.

Huang CC, Sugino K, Shima Y, Guo C, Bai S, Mensh BD, Nelson SB, Hantman AW (2013) Convergence of pontine and proprioceptive streams onto multimodal cerebellar granule cells. Elife 2:e00400.

Jakab RL, Hamori J (1988) Quantitative morphology and synaptology of cerebellar glomeruli in the rat. Anat Embryol (Berl) 179:81–88.

Ji Z, Hawkes R (1994) Topography of Purkinje cell compartments and mossy fiber terminal fields in lobules II and III of the rat cerebellar cortex: spinocerebellar and cuneocerebellar projections. Neuroscience 61:935–954.

Jiang J, Azim E, Ekerot CF, Alstermark B (2015) Direct and indirect spinocerebellar pathways: shared ideas but different functions in motor control. Front Comput Neurosci 9:75.

Kaneyama T, Shirasaki R (2018) Post-crossing segment of dI1 commissural axons forms collateral branches to motor neurons in the developing spinal cord. J Comp Neurol 526:1943–1961.

Kato S, Kobayashi K, Kobayashi K (2014) Improved transduction efficiency of a lentiviral vector for neuron-specific retrograde gene transfer by optimizing the junction of fusion envelope glycoprotein. J Neurosci Methods 227:151–158.

Kim JC, Cook MN, Carey MR, Shen C, Regehr WG, Dymecki SM (2009) Linking genetically defined neurons to behavior through a broadly applicable silencing allele. Neuron 63:305–315.

Liang H, Bacskai T, Paxinos G (2015) Termination of vestibulospinal fibers arising from the spinal vestibular nucleus in the mouse spinal cord. Neuroscience 294:206–214.

Llewellyn-Smith IJ, Martin CL, Fenwick NM, Dicarlo SE, Lujan HL, Schreihofer AM (2007) VGLUT1 and VGLUT2 innervation in autonomic regions of intact and transected rat spinal cord. J Comp Neurol 503:741–767.

Luo Y, Patel RP, Sarpong GA, Sasamura K, Sugihara I (2018) Single axonal morphology and termination to cerebellar aldolase C stripes characterize distinct spinocerebellar projection systems originating from the thoracic spinal cord in the mouse. J Comp Neurol 526:681–706.

Madisen L, Garner AR, Shimaoka D, Chuong AS, Klapoetke NC, Li L, van der Bourg A, Niino Y, Egolf L, Monetti C, Gu H, Mills M, Cheng A, Tasic B, Nguyen TN, Sunkin SM, Benucci A, Nagy A, Miyawaki A, Helmchen F, et al. (2015) Transgenic mice for intersectional targeting of neural sensors and effectors with high specificity and performance. Neuron 85:942–958.

Madisen L, Zwingman TA, Sunkin SM, Oh SW, Zariwala HA, Gu H, Ng LL, Palmiter RD, Hawrylycz MJ, Jones AR, Lein ES, Zeng H (2010) A robust and high-throughput Cre reporting and characterization system for the whole mouse brain. Nat Neurosci 13:133–140.

Malet M, Vieytes CA, Lundgren KH, Seal RP, Tomasella E, Seroogy KB, Hokfelt T, Gebhart GF, Brumovsky PR (2013) Transcript expression of vesicular glutamate transporters in lumbar dorsal root ganglia and the spinal cord of mice: effects of peripheral axotomy or hindpaw inflammation. Neuroscience 248:95–111.

Manni E, Petrosini L (2004) A century of cerebellar somatotopy: a debated representation. Nat Rev Neurosci 5:241–249.

Marr D (1969) A theory of cerebellar cortex. J Physiol 202:437–470.

Matsushita M, Gao X (1997) Projections from the thoracic cord to the cerebellar nuclei in the rat, studied by anterograde axonal tracing. J Comp Neurol 386:409–421.

Matsushita M, Hosoya Y (1979) Cells of origin of the spinocerebellar tract in the rat, studied with the method of retrograde transport of horseradish peroxidase. Brain Res 173:185–200.

Matsushita M, Ikeda M (1970) Spinal projections to the cerebellar nuclei in the cat. Exp Brain Res 10:501–511.

Matsushita M, Yaginuma H, Tanami T (1992) Somatotopic termination of the spino-olivary fibers in the cat, studied with the wheat germ agglutinin-horseradish peroxidase technique. Exp Brain Res 89:397–407.

Miura H, Quadros RM, Gurumurthy CB, Ohtsuka M (2018) Easi-CRISPR for creating knock-in and conditional knockout mouse models using long ssDNA donors. Nat Protoc 13:195–215.

Mogensen H, Bengtsson F, Jorntell H (2017) No medium-term spinocerebellar input plasticity in deep cerebellar nuclear neurons in vivo? Cerebellum 16:638–647.

Nanes BA (2015) Slide set: reproducible image analysis and batch processing with ImageJ. Biotechniques 59:269–278.

Ogujiofor OW, Pop IV, Espinosa F, Durodoye RO, Viacheslavov ML, Jarvis R, Landy MA, Gurumurthy CB, Lai HC (2021) An Atoh1 CRE knock-in mouse labels motor neurons involved in fine motor control. eNeuro 8: ENEURO.0221-20.2021.

Oldenbeuving AW, Eisenman LM, De Zeeuw CI, Ruigrok TJ (1999) Inferior olivary-induced expression of Fos-like immunoreactivity in the cerebellar nuclei of wild-type and Lurcher mice. Eur J Neurosci 11:3809–3822.

Oscarsson O (1965) Functional organization of the spino- and cuneocerebellar tracts. Physiol Rev 45:495–522.

Oscarsson O, Sjolund B (1977a) The ventral spino-olivocerebellar system in the cat: I. Identification of five paths and their termination in the cerebellar anterior lobe. Exp Brain Res 28:469–486.

Oscarsson O, Sjolund B (1977b) The ventral spine-olivocerebellar system in the cat: II. Termination zones in the cerebellar posterior lobe. Exp Brain Res 28:487–503.

Park YG, Sohn CH, Chen R, McCue M, Yun DH, Drummond GT, Ku T, Evans NB, Oak HC, Trieu W, Choi H, Jin X, Lilascharoen V, Wang J, Truttmann MC, Qi HW, Ploegh HL, Golub TR, Chen SC, Frosch MP, et al. (2018) Protection of tissue physicochemical properties using polyfunctional crosslinkers. Nat Biotechnol 37:73–83.

Paxinos G, Franklin KB (2007) The mouse brain in stereotaxic coordinates, Ed 3. San Diego: Academic.

Pivetta C, Esposito MS, Sigrist M, Arber S (2014) Motor-circuit communication matrix from spinal cord to brainstem neurons revealed by developmental origin. Cell 156:537–548.

Popova LB, Ragnarson B, Orlovsky GN, Grant G (1995) Responses of neurons in the central cervical nucleus of the rat to proprioceptive and vestibular inputs. Arch Ital Biol 133:31–45.

Quadros RM, Miura H, Harms DW, Akatsuka H, Sato T, Aida T, Redder R, Richardson GP, Inagaki Y, Sakai D, Buckley SM, Seshacharyulu P, Batra SK, Behlke MA, Zeiner SA, Jacobi AM, Izu Y, Thoreson WB, Urness LD, Mansour SL, et al. (2017) Easi-CRISPR: a robust method for one-step generation of mice carrying conditional and insertion alleles using long ssDNA donors and CRISPR ribonucleoproteins. Genome Biol 18:92.

Quinones HI, Savage TK, Battiste J, Johnson JE (2010) Neurogenin 1 (Neurog1) expression in the ventral neural tube is mediated by a distinct enhancer and preferentially marks ventral interneuron lineages. Dev Biol 340:283–292.

Reeber SL, Gebre SA, Sillitoe RV (2011) Fluorescence mapping of afferent topography in three dimensions. Brain Struct Funct 216:159–169.

Rodrigues DM, Li AY, Nair DG, Blennerhassett MG (2011) Glial cell line-derived neurotrophic factor is a key neurotrophin in the postnatal enteric nervous system. Neurogastroenterol Motil 23:e44–e56.

Rose MF, Ahmad KA, Thaller C, Zoghbi HY (2009) Excitatory neurons of the proprioceptive, interoceptive, and arousal hindbrain networks share a developmental requirement for Math1. Proc Natl Acad Sci USA 106:22462–22467.

Sakai N, Insolera R, Sillitoe RV, Shi SH, Kaprielian Z (2012) Axon sorting within the spinal cord marginal zone via Robo-mediated inhibition of N-cadherin controls spinocerebellar tract formation. J Neurosci 32:15377–15387.

Schindelin J, Arganda-Carreras I, Frise E, Kaynig V, Longair M, Pietzsch T, Preibisch S, Rueden C, Saalfeld S, Schmid B, Tinevez JY, White DJ, Hartenstein V, Eliceiri K, Tomancak P, Cardona A (2012) Fiji: an open-source platform for biological-image analysis. Nat Methods 9:676–682.

Sengul G, Fu Y, Yu Y, Paxinos G (2015) Spinal cord projections to the cerebellum in the mouse. Brain Struct Funct 220:2997–3009.

Shambes GM, Gibson JM, Welker W (1978) Fractured somatotopy in granule cell tactile areas of rat cerebellar hemispheres revealed by micromapping. Brain Behav Evol 15:94–140.

Sherrington CS (1906) The integrative action of the nervous system. New Haven, CT: Yale UP.

Sillitoe RV, Fu YH, Watson C (2012) The mouse nervous system (Watson C, Paxinos G, Puelles L, eds), Ed 1, pp 360–397. Amsterdam: Elsevier Academic.

Soriano P (1999) Generalized lacZ expression with the ROSA26 Cre reporter strain. Nat Genet 21:70–71.

Suzuki H, Hase A, Miyata Y, Arahata K, Akazawa C (1998) Prominent expression of glial cell line-derived neurotrophic factor in human skeletal muscle. J Comp Neurol 402:303–312.

Swenson RS, Castro AJ (1983a) The afferent connections of the inferior olivary complex in rats: a study using the retrograde transport of horseradish peroxidase. Am J Anat 166:329–341.

Swenson RS, Castro AJ (1983b) The afferent connections of the inferior olivary complex in rats: an anterograde study using autoradiographic and axonal degeneration techniques. Neuroscience 8:259–275.

Szabo T, Libouban S, Denizot JP (1990) A well defined spinocerebellar system in the weakly electric teleost fish *Gnathonemus petersii*: a tracing and immuno-histochemical study. Arch Ital Biol 128:229–247.

Trupp M, Ryden M, Jornvall H, Funakoshi H, Timmusk T, Arenas E, Ibanez CF (1995) Peripheral expression and biological activities of GDNF, a new neurotrophic factor for avian and mammalian peripheral neurons. J Cell Biol 130:137–148.

Tuthill JC, Azim E (2018) Proprioception. Curr Biol 28:R194–R203.

Watson C, Paxinos G, Kayalioglu G (2009) The spinal cord: a Christopher and Dana Reeve Foundation text and atlas. San Diego: Academic.

White JJ, Sillitoe RV (2017) Genetic silencing of olivocerebellar synapses causes dystonia-like behaviour in mice. Nat Commun 8:14912.

Wiksten B (1987) Further studies on the fiber connections of the central cervical nucleus in the cat. Exp Brain Res 67:284–290.

Wilson SI, Shafer B, Lee KJ, Dodd J (2008) A molecular program for contralateral trajectory: rig-1 control by LIM homeodomain transcription factors. Neuron 59:413–424.

Windhorst U (2007) Muscle proprioceptive feedback and spinal networks. Brain Res Bull 73:155–202.

Yang H, Xie X, Deng M, Chen X, Gan L (2010) Generation and characterization of Atoh1-Cre knock-in mouse line. Genesis 48:407–413.

Yuengert R, Hori K, Kibodeaux EE, McClellan JX, Morales JE, Huang TW, Neul JL, Lai HC (2015) Origin of a non-Clarke's column division of the dorsal spinocerebellar tract and the role of caudal proprioceptive neurons in motor function. Cell Rep 13:1258–1271.